arXiv:1412.5882v1 [cond-mat.str-el] 18 Dec 2014

Study of decoherence in models for hard-core bosons coupled to optical phonons

A. Dey, M. Q. Lone, and S. Yarlagadda
CMP Div., 1/AF Salt Lake, Saha Institute of Nuclear physics, Kolkata, India -700064
(Dated: December 19, 2014)

Understanding coherent dynamics of excitons, spins, or hard-core bosons (HCBs) has tremendous scientific and technological implications for light harvesting and quantum computation. Here, we study decay of excited-state population and decoherence in two models for HCBs, namely: an infinite-range HCB model governed by Markovian dynamics and a two-site HCB model with site-dependent strong potentials and subject to non-Markovian dynamics. Both models are investigated in the regimes of antiadiabaticity and strong HCB-phonon coupling with each site providing a different local optical phonon environment; furthermore, the HCB systems in both models are taken to be initially uncorrelated with the environment in the polaronic frame of reference. For the infinite-range model, we derive an effective many-body Hamiltonian that commutes with the long-range system Hamiltonian and thus has the same set of eigenstates; consequently, a quantum-master-equation approach shows that the quantum states of the system do not decohere. In the case of the two-site HCB model, we show clearly that the degree of decoherence and decay of excited state are enhanced by the proximity of the site-energy difference to the eigenenergy of phonons and are most pronounced when the site-energy difference is at resonance with twice the polaronic energy; additionally, the decoherence and the decay effects are reduced when the strength of HCB-phonon coupling is increased. Even for a multimode situation, the degree of decoherence and decay are again dictated by the nearness of the energy difference to the allowed phonon mode eigenenergies.

PACS numbers: 71.38.-k, 03.65.Yz, 85.35.Be, 87.10.Hk

I. INTRODUCTION

Quantum information processing heavily relies on a precious and fragile resource, namely, quantum entanglement [1]. The fragility of entanglement is due to the coupling between a quantum system and its environment; such a coupling leads to decoherence, the process by which information is degraded. Decoherence is the fundamental mechanism by which fragile superposition of states is destroyed thereby producing a quantum to classical transition [2, 3]. Since coupling of a quantum system to the environment and the concomitant entanglement fragility are ubiquitous [1, 2], it is imperative that progress be made in minimizing decoherence.

In general, a many-qubit (i.e., many-particle) system can have distance-dependent interaction. The two limiting cases for interaction are particle (HCB) hopping strength that is independent of distance and a system with nearest-neighbor hopping only. In this work, we consider an extreme model involving distance-independent interaction of HCBs which can be mapped onto the following spin-model: $\sum_{i,j>i}[-J_\perp(S_i^xS_j^x + S_i^yS_j^y) + J_\parallel S_i^zS_j^z]$. Such a model has relevance to many realistic physical systems of interest. Firstly, the well-studied Lipkin-Meshkov-Glick (LMG) model [4] $H_{\rm LMG} = -2h(\sum_j S_j^z) - 2\lambda[(\sum_j S_j^x)^2 + \gamma(\sum_j S_j^y)^2]/N$ (for $h = 0$ and $\gamma = 1$) is a special case of the above mentioned long-range model (for $J_\parallel = 0$ and $J_\perp = \lambda$); while, for $h = 0$ and $\gamma = 0$, LMG model is a special case of the model for $J_\perp = 0$ and $J_\parallel = -\lambda$. Long-range interactions can actually occur quite naturally in cavity quantum electrodynamics; by varying the external model parameters, it has been proposed that positive and negative values of λ as well as $-1 \le \gamma \le 1$ values can be achieved [5]. Secondly, it has been shown by Ezawa that the long-range ferromagnetic Heisenberg model describes well a zigzag graphene nanodisc [6]. A two-spin system and a four-spin system (with spins at the corners of a regular tetrahedron) can be physically realized (for instance from a Hubbard model) as exact special cases of the long-range model; it is conceivable that slightly larger clusters of particles (for instance, clusters containing 6 or 8 particles) can be physically realized as reasonable approximations of such a model.

Highly efficient coherent energy transfer processes in light-harvesting complexes is an active area of research [7]. Two-dimensional electronic spectroscopy gives a picture of the evolution of the density matrix and enables mapping of populations and coherences [8]. Fully connected network (FCN) is a well-studied model in the context of excitation energy transfer (EET) in Fenna-Matthews-Olson (FMO) complexes [9]. FCN is characterized by uniform hopping strength between any pair of sites (chromophores in the case of FMO complexes) and is an extreme limit of long-range interaction model for excitons. Moreover, the phonon fluctuations at various sites (chromophores) are uncorrelated to each other [8], i.e., local phonon effects are significant in such complexes. The system-bath coupling in photosynthetic complexes is thought to be not weak but to be at least in the intermediate regime [8]; instead of employing the usual quantum master equation techniques valid for the weak-coupling limit, modified approaches valid for broader range of couplings have been studied.

Modelling and controlling the environment of a solid-state quantum bit is a major challenge in quantum computation. Fairly long coherence times have been achieved

in semiconductor-based double quantum dots where the qubit information is encoded in the singlet-triplet states of two spins with total S^z equal to zero [10]. In these quantum dot systems, spin states are prepared, manipulated, and measured using rapid control of Heisenberg exchange interaction. However, the small size of a semiconductor qubit is limited by the extent of the electronic wavefunction which is more than a few nanometers.

In this work, without specifically modelling either a light-harvesting system or a qubit device, we would like to identify and understand some important features of related HCB systems which lead to either insignificant or sufficiently weak decoherence and decay of excited-state population. To this end, in the regimes of strong HCB-phonon interaction and antiadiabaticity, we study two HCB models in the polaronic frame of reference where initially the system and the environment constitute a simply separable state. In the transformed polaronic frame, the interaction term is weak and enables use of perturbation theory; furthermore, both preparation and measurement can be done in the dressed (polaronic) basis [11, 12]. We first analyze the nature of decoherence and decay of excited-state population in an infinite-range interaction model for HCBs that are coupled to local optical phonons. We show that the effective Hamiltonian in second-order perturbation theory retains the same eigenstates as the infinite-range system Hamiltonian. Our dynamical analysis shows that the system, when Markov processes are considered, neither decoheres nor allows decay of excited states. Next, for the more realistic situation where lattice sites have different site-energies and the dynamics is non-Markovian, (instead of a many-body problem) we analyze a more tractable case where just one HCB is hopping between two sites and the HCB-phonon coupling is local. Using non-Markovian second-order quantum master equation, we find that decoherence as well as decay of the population of the excited state are small if the site-energy difference is sufficiently different from the phonon eigenenergies; these features are manifested for both single-mode and multimode optical phonons.

The rest of the paper is organized as follows. In Sec. II, we introduce the infinite-range HCB Hamiltonian strongly coupled to local optical phonons and derive the effective Hamiltonian. In Sec. III, using the master-equation approach, we study decoherence under Markovian dynamics. Next, in Sec. IV, we study decoherence and decay of excited state using a non-Markovian analysis for a system of two sites (each with a different site energy). Finally, in Sec. V, we give our conclusions and make some general remarks regarding the wider context of our results. The paper also has an appendix containing detailed calculations for the terms of the master equation used for the two-site case.

II. INFINITE-RANGE HCB MODEL WITH HCBS COUPLED TO LOCAL OPTICAL PHONONS

We begin by introducing the infinite-range HCB model whose decoherence will be studied when the system is coupled to local phonons. The Hamiltonian for that is defined as:

$$H_{\rm HCB} = \sum_{i,j>i} [\frac{-J_\perp}{2}(b_i^\dagger b_j + \text{H.c.}) + J_\parallel (n_i - \frac{1}{2})(n_j - \frac{1}{2})], \tag{1}$$

where $\frac{J_\perp}{2}$ and $J_\parallel$ ($J_\perp > 0$ and $J_\parallel > 0$) are the hopping and HCB repulsion strengths between different sites, respectively. HCB creation and destruction operators are defined as $b_i^\dagger$ and b_i with the commutation relations given by

$$\begin{aligned} [b_i, b_j] = [b_i, b_j^\dagger] = 0, \text{ for } i \neq j, \\ \{b_i, b_i^\dagger\} = 1, \end{aligned} \tag{2}$$

and $n_i \equiv b_i^\dagger b_i$. In Eq. (1), it is understood that $J_\perp = J_\perp^\star/(N-1)$ and $J_\parallel = J_\parallel^\star/(N-1)$ (where $J_\perp^\star$ and $J_\parallel^\star$ are finite quantities) so that the energy per site remains finite as $N \to \infty$. The total Hamiltonian is defined by

$$\begin{aligned} H_T = \sum_{i,j>i} [\frac{-J_\perp}{2}(b_i^\dagger b_j + \text{H.c.}) + J_\parallel (n_i - \frac{1}{2})(n_j - \frac{1}{2})] \\ + \omega \sum_j a_j^\dagger a_j + g\omega \sum_j (n_j - \frac{1}{2})(a_j + a_j^\dagger), \end{aligned} \tag{3}$$

where a_j and $a_j^\dagger$ are the destruction and creation operators of phonons, respectively, g is the HCB-phonon coupling constant, and ω is the phonon frequency. Subsequently, we perform the well-known Lang-Firsov (LF) transformation [13, 14] on this Hamiltonian. Under the LF transformation given by

$$H_T^L \equiv e^S H_T e^{-S} = H_0^L + H_I^L, \tag{4}$$

with $S = -g\sum_i (n_i - \frac{1}{2})(a_i - a_i^\dagger)$, the operators b_j and a_j transform like fermions and bosons. Next, the unperturbed Hamiltonian H_0^L is expressed as [14]

$$H_0^L = H_s^L + H_{env}^L, \tag{5}$$

where we identify H_s^L as the system Hamiltonian

$$\begin{aligned} H_s^L = \sum_{i,j>i} [\frac{-J_\perp}{2} e^{-g^2}(b_i^\dagger b_j + \text{H.c.}) \\ + J_\parallel (n_i - \frac{1}{2})(n_j - \frac{1}{2})], \end{aligned} \tag{6}$$

and H_{env}^L as the Hamiltonian of the environment

$$H_{env}^L = \omega \sum_j a_j^\dagger a_j. \tag{7}$$

On the other hand, the interaction H_I^L which we will treat as perturbation is given by

$$H_I^L = \frac{-J_\perp}{2} e^{-g^2} \sum_{i,j>i} [b_i^\dagger b_j] \{ \mathcal{S}_+^{ij\,\dagger} \mathcal{S}_-^{ij} - 1 \} + \text{H.c.}, \quad (8)$$

where $\mathcal{S}_\pm^{ij} = \exp[\pm g(a_i - a_j)]$. In the transformed frame, the system Hamiltonian H_s^L depicts that all the HCBs are coupled to the same phononic mean-field. Thus, the unperturbed Hamiltonian H_0^L comprises of the system Hamiltonian H_s^L representing HCBs with the same reduced hopping term $\frac{1}{2} J_\perp e^{-g^2}$ and the environment Hamiltonian H_{env}^L involving displaced bath oscillators corresponding to local distortions. Here it should be pointed out that the mean-field term H_s^L involves controlled degrees of freedom. Thus no irreversibility is involved under evolution due to H_0^L. *On the other hand, perturbation H_I^L pertains to the interaction of HCBs with local deviations from the phononic mean-field; the interaction term H_I^L represents numerous or uncontrolled environmental degrees of freedom and thus has the potential for producing decoherence.* Furthermore, it is of interest to note that the interaction term is weak in the transformed frame unlike the interaction in the original frame; thus one can perform perturbation theory with the interaction term. We represent the eigenstates of the unperturbed Hamiltonian H_0^L as $|n,m\rangle \equiv |n\rangle_s \otimes |m\rangle_{ph}$ with the corresponding eigenenergies $E_{n,m} = E_n^s + E_m^{ph}$; $|n\rangle_s$ is the eigenstate of the system with eigenenergy E_n^s while $|m\rangle_{ph}$ is the eigenstate for the environment with eigenenergy E_m^{ph}. Henceforth, for brevity, we will use $\omega_m \equiv E_m^{ph}$. On observing that $\langle 0,0|H_I^L|0,0\rangle = 0$ (i.e., the ground state expectation value of the deviations is zero), we obtain the next relevant second-order perturbation term [14]

$$E^{(2)} = \sum_{n,m} \frac{\langle 0,0|H_I^L|n,m\rangle\langle n,m|H_I^L|0,0\rangle}{E_{0,0} - E_{n,m}}. \quad (9)$$

For strong coupling (i.e., $g^2 \gg 1$) [15] and non-adiabatic (i.e., $J_\perp^\star/\omega \leq 1$) [16] conditions assumed in this paper, it follows that $J_\perp^\star e^{-g^2} \ll \omega$. On noting that $\omega_m - \omega_0 = \omega_m$ is a positive integral multiple of ω and that $E_n^s - E_0^s \leq J_\perp^\star e^{-g^2}$ (as shown in the next section), we get the following second-order term $H^{(2)}$ [17] using Schrieffer-Wolff (SW) transformation (as elaborated in Appendix A of Refs. 18 and 19):

$$\begin{aligned} H^{(2)} &= -\sum_m \frac{{}_{ph}\langle 0|H_I|m\rangle_{ph}\ {}_{ph}\langle m|H_I|0\rangle_{ph}}{\omega_m} \\ &= \sum_{i,j>i} \Big[\Big(\frac{1}{2} J_\perp^{(2)} b_i^\dagger b_j + \text{H.c.} \Big) \\ &\qquad - \frac{1}{2} J_\parallel^{(2)} \{ n_i(1-n_j) + n_j(1-n_i) \} \Big], \quad (10) \end{aligned}$$

where

$$J_\perp^{(2)} \equiv -(N-2) f_1(g) \frac{J_\perp^2 e^{-2g^2}}{2\omega} \sim -(N-2) \frac{J_\perp^2 e^{-g^2}}{2g^2\omega}, \quad (11)$$

$$J_\parallel^{(2)} \equiv [2f_1(g) + f_2(g)] \frac{J_\perp^2 e^{-2g^2}}{2\omega} \sim \frac{J_\perp^2}{4g^2\omega}, \quad (12)$$

with $f_1(g) \equiv \sum_{l=1}^\infty g^{2l}/(l!l)$ and $f_2(g) \equiv \sum_{j=1}^\infty \sum_{l=1}^\infty g^{2(j+l)}/[j!l!(j+l)]$. The effective Hamiltonian $H_s^L + H^{(2)}$ is a low energy Hamiltonian obtained by the canonical SW transformation [20, 21] decoupling the low-energy and the high-energy subspaces; this decoupling is a consequence of $J_\perp^\star e^{-g^2} \ll \omega$. We now make the important observation that the effective Hamiltonian $H_s^L + H^{(2)}$ has the same set of eigenstates as those of H_s^L and H_{HCB} because $\sum_{i,j>i}(n_i - \frac{1}{2})(n_j - \frac{1}{2})$ commutes with both H_s^L and H_{HCB}. Actually, we have shown that even in higher-order perturbation theory (higher than second order) the eigenstates of the effective Hamiltonian do not change [22]. The small parameter of our perturbation theory, for a small N system, is $\frac{J_\perp}{g\omega}$ (see Ref. 23 for details); whereas for a large N, the small parameter is $\frac{J_\perp^\star}{g^2\omega}$ (see Ref. 24 for an explanation). It is the long range of the model that enables the eigenstates of the system to remain unchanged. While the fact that the eigenstates of the effective Hamiltonian remain the same as those of H_{HCB} may be suggestive of the robustness of the states of this long-range model, to establish that the states of the system are actually decoherence free, it is necessary to show that the off-diagonal matrix elements of the system's reduced density matrix do not diminish. Next, we study decoherence in a dynamical context and gain more insight into how the states of our H_{HCB} can be decoherence free.

III. DYNAMICAL EVOLUTION OF THE SYSTEM

In this section, we will study decoherence in the system from the dynamical perspective. We will discuss the dynamics of an open quantum system, described by the H_{HCB}, using master equation approach. Our quantum system is open because it is coupled to another quantum system, i.e., a bath or environment [25]. In our case, H_{HCB} is coupled to a bath of local optical phonons [see Eq. (3)]. As a consequence of the system-environment coupling, the state of the system may change. This interaction may lead to certain system-environment correlations such that the resulting state of the system may no longer be represented in terms of unitary Hamiltonian dynamics. The dynamics of the system, described by the reduced density matrix $\rho_s(t)$ at time t, is obtained from the density matrix $\rho_T(t)$ of the total system by taking the partial trace over the degrees of freedom of the environment:

$$\rho_s(t) = Tr_R\left[\rho_T(t)\right] = Tr_R\left[U(t)\rho_T(0)U^\dagger(t)\right], \quad (13)$$

where $U(t)$ represents the time-evolution operator of the total system. Now it is evident from the above equation that we need first to determine the dynamics

of the total system which is a difficult task in most of the cases. By contrast, master equation approach conveniently and directly yields the time evolution of the reduced density matrix of the system interacting with an environment. This approach relieves us from the need of having to first determine the dynamics of the total system-environment combination and then to trace out the degrees of freedom of the environment.

We begin by observing that, to understand decoherence in the original frame of reference where the HCB-phonon coupling is strong, it is convenient to use the LF transformed frame of reference: in the LF frame the system-environment coupling is weak, and furthermore, a polaron (represented by $e^{-S}b^\dagger|0\rangle_s \otimes |0\rangle_{ph}$) that is entangled with the environment in the original frame of reference becomes unentangled in the LF frame (i.e., it becomes an undressed particle represented by $b^\dagger|0\rangle_s \otimes |0\rangle_{ph}$). The relevant Hamiltonian (for our decoherence analysis) is the following LF transformed Hamiltonian:

$$H_T^{\rm L} = H_0^L + H_I^L, \tag{14}$$

where H_0^L is the system-environment Hamiltonian given by Eq. (5) and H_I^L represents the interaction Hamiltonian given by Eq. (8). It is convenient and simple to derive the quantum master equation in the interaction picture. Thus our starting point is the interaction picture von Neumann equation for the total density operator $\tilde{\rho}_T(t)$

$$\frac{d\tilde{\rho}_T(t)}{dt} = -i[\tilde{H}_I^L(t), \tilde{\rho}_T(t)], \tag{15}$$

where $\tilde{H}_I^L(t) = e^{iH_0^L t}H_I^L e^{-iH_0^L t}$ and $\tilde{\rho}_T(t) = e^{iH_0^L t}\rho_T(t)e^{-iH_0^L t}$ are the interaction Hamiltonian and the total system density matrix operators (respectively) expressed in the interaction picture. Re-expressing the above equation in integral form yields

$$\tilde{\rho}_T(t) = \tilde{\rho}_T(0) - i\int_0^t d\tau[\tilde{H}_I^L(\tau), \tilde{\rho}_T(\tau)]. \tag{16}$$

Nowadays there is considerable interest in systems with initial correlation with the environment [26, 27]. Here too the initial state of the total system, in the original untransformed frame of reference, is taken to be made up of particles entangled with the environment (i.e., polarons or particles dressed with environmental phonons), so that in the LF frame the initial state transforms to a factorized (or simply separable) state given as $\rho_T(0) = \rho_s(0) \otimes R_0$ with $R_0 = \sum_n |n\rangle_{ph\,ph}\langle n|e^{-\beta\omega_n}/Z$ being the initial thermal density matrix operator of the environment and temperature being equal to $\frac{1}{k_B\beta}$; furthermore, $Z = \sum_n e^{-\beta\omega_n}$ defines the partition function of the environment. Here it should be pointed out that states can be prepared and measured in the dressed (polaronic) basis; the dressed (polaronic) basis can be used for input and output [11]. The possible preparation of this initial factorized state is discussed for a realistic system, i.e., the double quantum dot (DQD) in Ref. 12. Moreover, if the phonon deformation time scale is much smaller than the bare hopping time scale (which is justified in strong coupling and non-adiabatic limit), the initial separability condition is certainly achievable. More specifically, in such a limit, as soon as a particle is put at any site, the local phonons quickly respond and reorganize to a new equilibrium position; consequently, the separable initial state (in the polaronic frame of reference) is formed. With this assumed initial state, we substitute Eq. (16) inside the commutator of Eq. (15) and then take the trace over the environmental degrees of freedom to obtain the following equation:

$$\frac{d\tilde{\rho}_s(t)}{dt} = -i\,Tr_R[\tilde{H}_I^L(t), \tilde{\rho}_s(0)\otimes R_0] - \int_0^t d\tau Tr_R[\tilde{H}_I^L(t), [\tilde{H}_I^L(\tau), \tilde{\rho}_T(\tau)]]. \tag{17}$$

The above equation still contains the total density matrix $\tilde{\rho}_T(\tau)$; in order to evaluate it, we rely on an approximation known as the Born approximation. This approximation assumes that the environment degrees of freedom are large and thus the effect on the environment due to the system is negligibly small for a weak system-environment coupling. As a consequence, we write $\tilde{\rho}_T(\tau) = \tilde{\rho}_s(\tau)\otimes R_0 + \mathcal{O}(\tilde{H}_I)$ within the second-order perturbation in system-environment interaction [25, 28–36]. Therefore we can write Eq. (17) in time-local form as

$$\frac{d\tilde{\rho}_s(t)}{dt} = -i\,Tr_R[\tilde{H}_I^L(t), \rho_s(0)\otimes R_0] - \int_0^t d\tau Tr_R[\tilde{H}_I^L(t), [\tilde{H}_I^L(\tau), \tilde{\rho}_s(t)\otimes R_0]]. \tag{18}$$

We note here that, for obtaining the non-Markovian time-convolutionless master equation (18), we replaced $\tilde{\rho}_s(\tau)$ with $\tilde{\rho}_s(t)$. This replacement is equivalent to obtaining a time-convolutionless master equation perturbatively up to only second order in the interaction Hamiltonian using the time-convolutionless projection operator technique [25, 32, 33]. It has been shown in a number of cases that time-local approach works better than time-nonlocal approach [25, 30, 34, 35, 37]. Now we will consider the second-order, time-convolutionless master equation (18) with the time variable τ replaced by $(t-\tau)$.

$$\frac{d\tilde{\rho}_s(t)}{dt} = -i\,Tr_R[\tilde{H}_I^L(t), \rho_s(0)\otimes R_0] - \int_0^t d\tau Tr_R[\tilde{H}_I^L(t), [\tilde{H}_I^L(t-\tau), \tilde{\rho}_s(t)\otimes R_0]]. \tag{19}$$

Next, we will study the Markovian dynamics of the system. To this end we assume that the correlation time scale τ_c for the environmental fluctuations is negligibly small compared to the relaxation time scale τ_s for the system, i.e., $\tau_c \ll \tau_s$. This time scale assumption is motivated by the condition $J^\star e^{-g^2} \ll \omega$ already mentioned in

Sec. 2. The Markov approximation ($\tau_c \ll \tau_s$) allows us to set the upper limit of the integral to ∞ in Eq. (19). Thus we obtain the second-order time-convolutionless Markovian master equation (see Ref. 25 for further details):

$$\frac{d\tilde{\rho}_s(t)}{dt} = -i\ Tr_R[\tilde{H}_I^L(t), \rho_s(0)\otimes R_0] - \int_0^\infty d\tau Tr_R[\tilde{H}_I^L(t), [\tilde{H}_I^L(t-\tau), \tilde{\rho}_s(t)\otimes R_0]]. \quad (20)$$

Defining $\{|n\rangle_{ph}\}$ as the basis set for phonons, therefore, we can write the master equation as:

$$\frac{d\tilde{\rho}_s(t)}{dt} = -i\sum_n {}_{ph}\langle n|[\tilde{H}_I^L(t), \rho_s(0)\otimes R_0]|n\rangle_{ph} - \sum_n \int_0^\infty d\tau \Big[{}_{ph}\langle n|\tilde{H}_I^L(t)\tilde{H}_I^L(t-\tau)\tilde{\rho}_s(t)\otimes R_0|n\rangle_{ph} - {}_{ph}\langle n|\tilde{H}_I^L(t)\tilde{\rho}_s(t)\otimes R_0\tilde{H}_I^L(t-\tau)|n\rangle_{ph} - {}_{ph}\langle n|\tilde{H}_I^L(t-\tau)\tilde{\rho}_s(t)\otimes R_0\tilde{H}_I^L(t)|n\rangle_{ph} + {}_{ph}\langle n|\tilde{\rho}_s(t)\otimes R_0\tilde{H}_I^L(t-\tau)\tilde{H}_I^L(t)|n\rangle_{ph}\Big]. \quad (21)$$

In order to simplify the above master equation, we need to evaluate the time evolution of the operators involved in H_I^L. Considering the second term in Eq. (21) yields

$$\begin{aligned} &{}_{ph}\langle n|\tilde{H}_I^L(t)\tilde{H}_I^L(t-\tau)\tilde{\rho}_s(t)\otimes R_0|n\rangle_{ph} \\ &= \sum_m e^{iH_s^L t}\,{}_{ph}\langle n|H_I^L|m\rangle_{ph} e^{-iH_s^L t}\ e^{iH_s^L(t-\tau)} \\ &\times {}_{ph}\langle m|H_I^L|n\rangle_{ph} e^{-iH_s^L(t-\tau)}\tilde{\rho}_s(t)\frac{e^{-\beta\omega_n}}{Z}e^{i(\omega_n-\omega_m)\tau}. \end{aligned} \quad (22)$$

We connect the HCBs in real space with those in momentum space as: $b_j^\dagger = \frac{1}{\sqrt{N}}\sum_{k_1} e^{ik_1 r_j}\ b_{k_1}^\dagger$ and $b_j = \frac{1}{\sqrt{N}}\sum_{k_1} e^{-ik_1 r_j}\ b_{k_1}$; henceforth, in momentum space, the creation and destruction operators of HCBs shall be denoted, respectively, as $b_{k_n}^\dagger$ and b_{k_n} with $n = 1, 2, 3, ...$ Then, it is important to note that the hopping term in the system Hamiltonian can be written as (see Refs. 17 and 38):

$$\begin{aligned} \frac{1}{2}J_\perp e^{-g^2}\sum_{i,j>i}(b_i^\dagger b_j + \text{H.c.}) &= \frac{1}{2}J_\perp e^{-g^2}\left[\sum_{i,j} b_i^\dagger b_j - \sum_i b_i^\dagger b_i\right] \\ &= \frac{1}{2}J_\perp e^{-g^2}\left[N\hat{n}_0 - \hat{N}_p\right] \\ &= \sum_{k_1}\epsilon_{k_1} b_{k_1}^\dagger b_{k_1}, \end{aligned} \quad (23)$$

where $J_\perp = J_\perp^\star/(N-1)$, $\hat{N}_p \equiv \sum_{k_1} b_{k_1}^\dagger b_{k_1}$ and $\hat{n}_0 \equiv b_0^\dagger b_0$ (i.e., the particle number in momentum $k_1 = 0$ state). Thus the single particle energy is given by

$$\epsilon_{k_1} = \frac{1}{2}J_\perp^\star\frac{N}{N-1}e^{-g^2}\delta_{k_1,0} - \frac{1}{2}J_\perp e^{-g^2}. \quad (24)$$

We take the total number of HCBs to be conserved; then, only the hopping term in H_s^L will contribute to the particle excitation energy [see Eq. (6)]. Thus, in Eq. (9), the largest value of the system excitation energy in the denominator is the maximum single particle excitation energy given by

$$E_n^s - E_0^s = \frac{1}{2}J_\perp^\star\frac{N}{N-1}e^{-g^2}, \quad (25)$$

which is N times the hopping term $(1/2)J_\perp e^{-g^2}$ in H_s^L. Let $\{|q\rangle_s\}$ denote the complete set of energy eigenstates (with eigenenergies E_q^s) of the system Hamiltonian H_s^L; then we can write:

$$e^{iH_s^L t}H_I^L e^{-iH_s^L t} = \frac{1}{2}J_\perp e^{-g^2}\sum_{l,j>l}\sum_{q,q'}|q\rangle_{ss}\langle q|e^{iH_s^L t}\left[\frac{1}{N}\sum_{k_1,k_2} b_{k_1}^\dagger b_{k_2} e^{i(k_1 r_l - k_2 r_j)}\right] e^{-iH_s^L t}|q'\rangle_{ss}\langle q'|\{\mathcal{S}_+^{lj\,\dagger}\mathcal{S}_-^{lj} - 1\} + \text{H.c.}, \quad (26)$$

which implies

$$e^{iH_s^L t}\ {}_{ph}\langle n|H_I^L|m\rangle_{ph} e^{-iH_s^L t} = \sum_{q,q'} |q\rangle_{ss}\langle q|\ {}_{ph}\langle n|H_I^L|m\rangle_{ph}|q'\rangle_{ss}\langle q'|e^{i(E_q^s - E_{q'}^s)t}, \tag{27}$$

where $|E_q^s - E_{q'}^s| \leq \frac{1}{2}J_\perp^\star(\frac{N}{N-1})e^{-g^2}$ [based on Eq. (25)]. Substituting Eq. (27) in Eq. (22), we get

$$\begin{aligned}
&{}_{ph}\langle n|\tilde{H}_I^L(t)\tilde{H}_I^L(t-\tau)\tilde{\rho}_s(t)\otimes R_0|n\rangle_{ph} \\
&= \sum_m \sum_{q,q',q''} \Big[|q\rangle_{ss}\langle q|\ {}_{ph}\langle n|H_I^L|m\rangle_{ph}|q'\rangle_{ss}\langle q'|\ {}_{ph}\langle m|H_I^L|n\rangle_{ph}|q''\rangle_{ss}\langle q''|e^{i[(E_q^s - E_{q'}^s)t + (E_{q'}^s - E_{q''}^s)(t-\tau)]}\Big]\tilde{\rho}_s(t)\frac{e^{-\beta\omega_n}}{Z}e^{i(\omega_n-\omega_m)\tau}.
\end{aligned} \tag{28}$$

Based on the above equation, at the temperature of 0 K, we get the following:

$$\begin{aligned}
&\sum_n {}_{ph}\langle n|\tilde{H}_I^L(t)\tilde{H}_I^L(t-\tau)\tilde{\rho}_s(t)\otimes R_0|n\rangle_{ph} \\
&= \sum_m \sum_{q,q',q''} \left[|q\rangle_{ss}\langle q|\ {}_{ph}\langle 0|H_I^L|m\rangle_{ph}|q'\rangle_{ss}\langle q'|\ {}_{ph}\langle m|H_I^L|0\rangle_{ph}|q''\rangle_{ss}\langle q''|e^{i[(E_q^s - E_{q'}^s)t + (E_{q'}^s - E_{q''}^s)(t-\tau)]}\right]\tilde{\rho}_s(t)e^{-i\omega_m\tau}.
\end{aligned} \tag{29}$$

Since $J_\perp^\star e^{-g^2} \ll \omega$ and since the maximum value of $|E_{q'}^s - E_{q''}^s| \leq J_\perp^\star e^{-g^2}$ as well as the maximum value of $|E_q^s - E_{q'}^s| \leq J_\perp^\star e^{-g^2}$, the following are valid approximations:

$$e^{i(t-\tau)[\omega_m + (E_{q'}^s - E_{q''}^s)]} \approx e^{i(t-\tau)\omega_m}, \tag{30}$$

and

$$e^{it[-\omega_m + (E_q^s - E_{q'}^s)]} \approx e^{-it\omega_m}, \tag{31}$$

where ω_m is a positive integral multiple of ω. The above approximations imply that we do not get terms producing decay. Then, on using the approximations given by Eqs. (30) and (31), Eq. (29) simplifies to be

$$\begin{aligned}
&\sum_n {}_{ph}\langle n|\tilde{H}_I^L(t)\tilde{H}_I^L(t-\tau)\tilde{\rho}_s(t)\otimes R_0|n\rangle_{ph} \\
&= \sum_m {}_{ph}\langle 0|H_I^L|m\rangle_{ph}\ {}_{ph}\langle m|H_I^L|0\rangle_{ph}\ \tilde{\rho}_s(t)e^{-i\omega_m\tau}.
\end{aligned} \tag{32}$$

Carrying out the same analysis on the remaining (i.e., third, fourth, and fifth) terms in the master equation, we write Eq. (21) at 0 K temperature as:

$$\begin{aligned}
\frac{d\tilde{\rho}_s(t)}{dt} &= -i\sum_n\ {}_{ph}\langle n|[\tilde{H}_I^L(t), \tilde{\rho}_s(0)\otimes R_0]|n\rangle_{ph} \\
&\quad - \sum_m \int_0^\infty d\tau \Big[{}_{ph}\langle 0|H_I^L|m\rangle_{ph}\ {}_{ph}\langle m|H_I^L|0\rangle_{ph}\ \tilde{\rho}_s(t)e^{-i\omega_m\tau} - \ {}_{ph}\langle m|H_I^L|0\rangle_{ph}\ \tilde{\rho}_s(t)\ {}_{ph}\langle 0|H_I^L|m\rangle_{ph}e^{i\omega_m\tau} \\
&\qquad - \ {}_{ph}\langle m|H_I^L|0\rangle_{ph}\ \tilde{\rho}_s(t)\ {}_{ph}\langle 0|H_I^L|m\rangle_{ph}e^{-i\omega_m\tau} + \tilde{\rho}_s(t)\ {}_{ph}\langle 0|H_I^L|m\rangle_{ph}\ {}_{ph}\langle m|H_I^L|0\rangle_{ph}e^{i\omega_m\tau}\Big].
\end{aligned} \tag{33}$$

Next, we evaluate the first term in the above equation and show that it is zero at the temperature of 0 K. We observe that

$$\begin{aligned}
Tr_R[\tilde{H}_I^L(t)R_0] &= \sum_n\ {}_{ph}\langle n|\tilde{H}_I^L(t)R_0|n\rangle_{ph} \\
&= \frac{1}{2}Je^{-g^2}\sum_{l,j\neq l}\Big[e^{iH_s^L t}b_l^\dagger b_j e^{-iH_s^L t}\ {}_{ph}\langle 0|\{\mathcal{S}_+^{lj^\dagger}\mathcal{S}_-^{lj} - 1\}|0\rangle_{ph}\Big] \\
&= 0.
\end{aligned} \tag{34}$$

Thus, we have $\sum_n\ {}_{ph}\langle n|[\tilde{H}_I^L(t), \rho_s(0)\otimes R_0]|n\rangle_{ph} = 0$ and the master equation at 0 K temperature simplifies as:

$$\begin{aligned}
\frac{d\tilde{\rho}_s(t)}{dt} = -\sum_n \Big[\int_0^\infty d\tau\ e^{-i(\omega_n - i\eta)\tau}|{}_{ph}\langle 0|H_I^L|n\rangle_{ph}|^2\ \tilde{\rho}_s(t) + \int_0^\infty d\tau\ e^{i(\omega_n + i\eta)\tau}\ \tilde{\rho}_s(t)\ |{}_{ph}\langle 0|H_I^L|n\rangle_{ph}|^2 \\
- \int_{-\infty}^\infty d\tau\ e^{i\omega_n\tau}\ {}_{ph}\langle n|H_I^L|0\rangle_{ph}\ \tilde{\rho}_s(t)\ {}_{ph}\langle 0|H_I^L|n\rangle_{ph}\Big],
\end{aligned} \tag{35}$$

where $\eta \to +0$. Now, we know that $\int_{-\infty}^{\infty} d\tau e^{i\omega_n \tau} \propto \delta(\omega_n)$. Therefore, on using this relation and the fact that ${}_{ph}\langle 0|H_I^L|0\rangle_{ph} = 0$, the third term in Eq. (35) vanishes; hence, we get

$$\frac{d\tilde{\rho}_s(t)}{dt} = i \sum_n \left[\frac{|{}_{ph}\langle 0|H_I^L|n\rangle_{ph}|^2}{\omega_n} \tilde{\rho}_s(t) - \tilde{\rho}_s(t) \frac{|{}_{ph}\langle 0|H_I^L|n\rangle_{ph}|^2}{\omega_n} \right]. \tag{36}$$

Here it should be pointed out that the above simplified form for the master equation was possible due to the Markovian approximation made. Based on Eq. (10), we identify the term $-\sum_n \left[\frac{|{}_{ph}\langle 0|H_I^L|n\rangle_{ph}|^2}{\omega_n} \right]$ in the above equation to be the term $H^{(2)}$ obtained in second-order perturbation which together with H_s^L makes up the effective Hamiltonian (in second-order perturbation). On noting that $\tilde{\rho}_s(t) = e^{iH_s^L t} \rho_s(t) e^{-iH_s^L t}$ and that $H^{(2)}$ commutes with H_s^L (see section 2), it follows from Eq. (36) that

$$\frac{d\rho_s(t)}{dt} = -i \left[H_s^L + H^{(2)}, \rho_s(t) \right]. \tag{37}$$

The above Eq. (37) shows that the effective Hamiltonian $(H_s^L + H^{(2)})$ governs the unitary evolution of the reduced density matrix $\rho_s(t)$ with $\rho_s(t) = e^{-i(H_s^L + H^{(2)})t} \rho_s(0) e^{i(H_s^L + H^{(2)})t}$. Let $|n\rangle_s$ be the simultaneous eigenstate for $H^{(2)}$ and H_s^L with eigenvalues $E_n^{(2)}$ and E_n^s, respectively. Then, from the above Eq. (37) we get:

$${}_s\langle n|\rho_s(t)|m\rangle_s = e^{-i(E_n - E_m)t} \, {}_s\langle n|\rho_s(0)|m\rangle_s, \tag{38}$$

where $E_n = E_n^s + E_n^{(2)}$. Thus we see from the above equation that there is only a phase shift but no decoherence! Thus, up to second order in perturbation, the assumption $J_\perp^\star e^{-g^2} \ll \omega$, the long range of the model, and the Markov approximation ($\tau_c \ll \tau_s$) together have ensured that the system, with a fixed $\sum_i n_i$, does not decohere; furthermore, there is no change in the population ${}_s\langle n|\rho_s(t)|n\rangle_s$.

Extending the dynamical analysis to the non-Markovian case for a system with different site energies is difficult for a many-site and many-body situation; hence, in the next section, we restrict ourselves to a two-site system involving a single HCB.

IV. NON-MARKOVIAN ANALYSIS FOR A TWO-SITE CASE WITH DIFFERENT SITE ENERGIES

A. Single-mode case

Here we consider the case where one HCB is hopping between two sites each having its local phonon environment. Initially, for simplicity, we consider the baths and the interaction terms to involve only a single mode and ignore the wavenumber dependence. The model Hamiltonian is given by

$$\begin{aligned} H = {} & \varepsilon_1(n_1 - \frac{1}{2}) + \varepsilon_2(n_2 - \frac{1}{2}) - \frac{J_\perp}{2}(b_1^\dagger b_2 + b_2^\dagger b_1) \\ & + J_\parallel (n_1 - \frac{1}{2})(n_2 - \frac{1}{2}) + g\omega \sum_{i=1,2} (n_i - \frac{1}{2})(a_i + a_i^\dagger) \\ & + \omega \sum_{i=1,2} a_i^\dagger a_i, \end{aligned} \tag{39}$$

where ε_1 and ε_2 are the site energies. In the regime of strong electron-phonon coupling, we perform the LF transformation

$$H^L = e^S H e^{-S}, \tag{40}$$

where again $S = -\sum_i g(n_i - \frac{1}{2})(a_i - a_i^\dagger)$. We make our analysis in the polaronic frame of reference where the system Hamiltonian H_s^L, interaction Hamiltonian H_I^L and the displaced-phonon Hamiltonian H_B^L are given by

$$\begin{aligned} H_s^L = {} & \varepsilon_1(n_1 - \frac{1}{2}) + \varepsilon_2(n_2 - \frac{1}{2}) - \frac{J_\perp e^{-g^2}}{2}(b_1^\dagger b_2 + b_2^\dagger b_1) \\ & + J_\parallel (n_1 - \frac{1}{2})(n_2 - \frac{1}{2}), \end{aligned} \tag{41}$$

$$H_I^L = -\frac{1}{2}[J_\perp^+ b_1^\dagger b_2 + J_\perp^- b_2^\dagger b_1], \tag{42}$$

and

$$H_{env}^L = \omega \sum_{i=1,2} a_i^\dagger a_i, \tag{43}$$

respectively. In the above equations

$$J_\perp^\pm = J_\perp e^{\pm g[(a_2 - a_2^\dagger) - (a_1 - a_1^\dagger)]} - J_\perp e^{-g^2}, \tag{44}$$

and

$$J_\perp e^{-g^2} = {}_{ph}\langle 0|J_\perp e^{\pm g[(a_2 - a_2^\dagger) - (a_1 - a_1^\dagger)]}|0\rangle_{ph}. \tag{45}$$

The system Hamiltonian H_s^L represents HCB coupled to the mean-phonon field and $\frac{1}{2}J_\perp e^{-g^2}$ is the resulting renormalized hopping amplitude. In the subspace involving only one HCB and two sites, the two eigenstates of H_s^L are given by $\frac{1}{\sqrt{1+\chi_1^2}}(\chi_1|10\rangle + |01\rangle)$

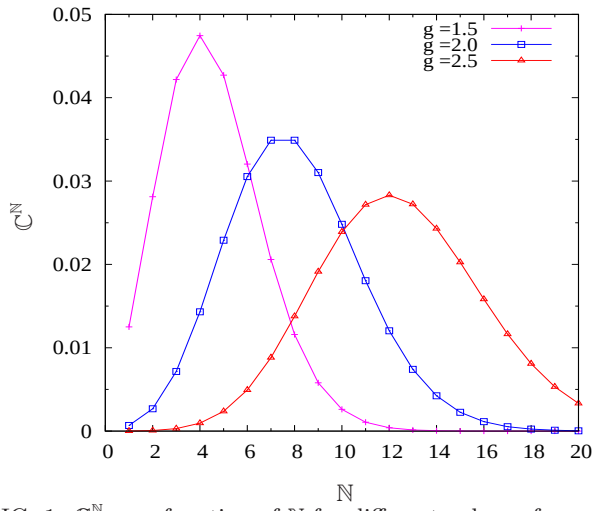

FIG. 1. $\mathbb{C}^{\mathbb{N}}$ as a function of $\mathbb{N}$ for different values of coupling g and for $\frac{J_\perp}{\omega} = 1.0$.

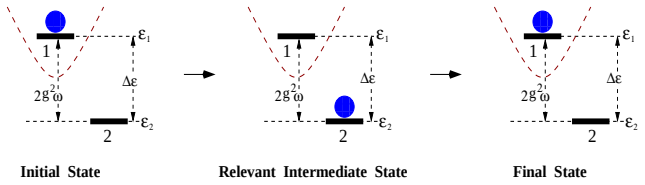

FIG. 2. Schematic representation of the site energies and hopping process leading to minimum coherence C(t) and maximum decay of excited state P(t); the intermediate state gives the dominant contribution. Here location of the HCB is given by the filled circle. Parabolic curve at site 1 depicts full distortion of the lattice environment at that site with corresponding energy $-g^2\omega$ $(+g^2\omega$) if the HCB is present (absent) at that site.

and $\frac{1}{\sqrt{1+\chi_2^2}}(\chi_2|10\rangle + |01\rangle)$ with corresponding eigenenergies $\frac{-J_\parallel - 2\sqrt{\Delta\varepsilon^2+J_\perp^2 e^{-2g^2}}}{4}$ and $\frac{-J_\parallel + 2\sqrt{\Delta\varepsilon^2+J_\perp^2 e^{-2g^2}}}{4}$, respectively; here, $\chi_1 = -\frac{\Delta\varepsilon - \sqrt{\Delta\varepsilon^2+J_\perp^2 e^{-2g^2}}}{J_\perp e^{-g^2}}$ and $\chi_2 = -\frac{\Delta\varepsilon + \sqrt{\Delta\varepsilon^2+J_\perp^2 e^{-2g^2}}}{J_\perp e^{-g^2}}$ with site-energy difference $\Delta\varepsilon = \varepsilon_1 - \varepsilon_2$. The interaction Hamiltonian H_I^L represents the HCBs coupled to fluctuations of local phonons around their mean-phonon field. As the interaction in the polaronic frame of reference is weak (compared to that in the original frame of reference), one can treat H_I^L as a perturbation. To analyze the non-Markovian dynamics of the model, we start with the simply separable initial state $\rho_T(0) = \rho_s(0) \otimes R_0$ where R_0 is the phonon density matrix at thermal equilibrium and is given by $R_0 = \sum_{n_1,n_2} |n_1,n_2\rangle_{ph}\,{}_{ph}\langle n_1,n_2|e^{-\beta\omega_{n_1,n_2}}/Z$. Here, n_1 and n_2 are the phonon occupation numbers at sites 1 and 2, respectively; henceforth, we will use the notation $|n\rangle_{ph} \equiv |n_1,n_2\rangle_{ph}$ and $\omega_n \equiv \omega_{n_1,n_2} = \omega(n_1+n_2)$.

Now, we start with the second-order, time-convolutionless (TCL), non-Markovian, quantum-master equation

$$\frac{d\tilde{\rho}_s(t)}{dt} = -\int_0^t d\tau Tr_R[\tilde{H}_I^L(t),[\tilde{H}_I^L(\tau),\tilde{\rho}_s(t)\otimes R_0]]. \quad (46)$$

At zero temperature, Eq. (46) can be rewritten as

$$\frac{d\tilde{\rho}_s(t)}{dt} = -\sum_m \int_0^t d\tau \Big[{}_{ph}\langle 0|\tilde{H}_I^L(t)|m\rangle_{ph}\,{}_{ph}\langle m|\tilde{H}_I^L(\tau)|0\rangle_{ph}\tilde{\rho}_s(t) - {}_{ph}\langle m|\tilde{H}_I^L(t)|0\rangle_{ph}\tilde{\rho}_s(t)_{ph}\langle 0|\tilde{H}_I^L(\tau)|m\rangle_{ph}$$
$$- {}_{ph}\langle m|\tilde{H}_I^L(\tau)|0\rangle_{ph}\tilde{\rho}_s(t)_{ph}\langle 0|\tilde{H}_I^L(t)|m\rangle_{ph} + \tilde{\rho}_s(t)_{ph}\langle 0|\tilde{H}_I^L(\tau)|m\rangle_{ph}\,{}_{ph}\langle m|\tilde{H}_I^L(t)|0\rangle_{ph}\Big]. \quad (47)$$

We choose the basis $\{|10\rangle,|01\rangle\}$ for our analysis and obtain the following useful expressions:

$$e^{-iH_s^L t}|10\rangle = [p(t)^*|10\rangle - i\kappa q(t)|01\rangle]e^{i\frac{J_\parallel}{4}t}, \quad (48)$$

and

$$e^{-iH_s^L t}|01\rangle = [p(t)|01\rangle - i\kappa q(t)|10\rangle]e^{i\frac{J_\parallel}{4}t}, \quad (49)$$

where $p(t) = \cos\left(t\sqrt{\frac{\Delta\varepsilon^2}{4}+\kappa^2}\right) + i\frac{\Delta\varepsilon}{2}\frac{\sin\left(t\sqrt{\frac{\Delta\varepsilon^2}{4}+\kappa^2}\right)}{\sqrt{\frac{\Delta\varepsilon^2}{4}+\kappa^2}}$, $q(t) = \frac{\sin\left(t\sqrt{\frac{\Delta\varepsilon^2}{4}+\kappa^2}\right)}{\sqrt{\frac{\Delta\varepsilon^2}{4}+\kappa^2}}$ and $\kappa = -\frac{J_\perp e^{-g^2}}{2}$. In addition, we also evaluate the matrix element

$${}_{ph}\langle 0|H_I^L|n\rangle_{ph} = \kappa(-1)^{n_1}\sqrt{C_n}\left(b_1^\dagger b_2 + (-1)^{n_1+n_2}b_2^\dagger b_1\right), \quad (50)$$

where $C_n = \frac{g^{2(n_1+n_2)}}{n_1!n_2!}$. Taking the matrix elements, with respect to $|10\rangle$ and $|01\rangle$, on both sides of Eq. (47) and by using Eqs. (48)–(50), we calculate the matrix elements of the four terms on the right hand side of Eq. (47) (details are shown in the Appendix). For the case when $|\Delta\varepsilon| \gg |\kappa|$, $|10\rangle$ and $|01\rangle$ are the approximate eigenstates of H_s^L. In this regime of parameter values, we ignore the ratio $\frac{|\kappa|}{|\Delta\varepsilon|}$ compared to 1 [in Eqs. (A2)–(A5)] and finally obtain simple form of the master equation for $\langle 10|\tilde{\rho}_s(t)|01\rangle$:

$$\frac{d\langle 10|\tilde{\rho}_s(t)|01\rangle}{dt} = -i\kappa^2 \sum_n{}' C_n \Big[\langle 10|\tilde{\rho}_s(t)|01\rangle \Big(\frac{e^{-i(\omega_n-\Delta\varepsilon)t}}{\omega_n-\Delta\varepsilon} - \frac{e^{i(\omega_n+\Delta\varepsilon)t}}{\omega_n+\Delta\varepsilon} - \frac{2\Delta\varepsilon}{\omega_n^2-\Delta\varepsilon^2}\Big) + \langle 01|\tilde{\rho}_s(t)|10\rangle(-1)^{n_1+n_2} e^{2i\Delta\varepsilon t}\Big(\frac{e^{i(\omega_n-\Delta\varepsilon)t}}{\omega_n-\Delta\varepsilon} - \frac{e^{-i(\omega_n+\Delta\varepsilon)t}}{\omega_n+\Delta\varepsilon} - \frac{2\Delta\varepsilon}{\omega_n^2-\Delta\varepsilon^2}\Big)\Big], \quad (51)$$

and its complex conjugate equation for $\langle 01|\tilde{\rho}_s(t)|10\rangle$. In the above equation, $\sum_n{}' \equiv \sum_{n_1,n_2}{}'$ excludes the case where n_1 and n_2 are simultaneously zero. Similarly, for the diagonal element $\langle 10|\tilde{\rho}_s(t)|10\rangle$, the differential equation can be written as

$$\frac{d\langle 10|\tilde{\rho}_s(t)|10\rangle}{dt} = -2\kappa^2 \sum_n{}' C_n \Big[\langle 10|\tilde{\rho}_s(t)|10\rangle \Big(\frac{\sin(\omega_n+\Delta\varepsilon)t}{\omega_n+\Delta\varepsilon} + \frac{\sin(\omega_n-\Delta\varepsilon)t}{\omega_n-\Delta\varepsilon}\Big) - \frac{\sin(\omega_n+\Delta\varepsilon)t}{\omega_n+\Delta\varepsilon}\Big]. \quad (52)$$

The above Eq. (52) is a first-order, non-homogeneous, differential equation; its solution is given by

$$\begin{aligned}\langle 10|\rho_s(t)|10\rangle = {} & \langle 10|\rho_s(0)|10\rangle \exp\Big[-2\kappa^2 \sum_n{}' C_n \Big(\frac{1-\cos(\omega_n+\Delta\varepsilon)t}{(\omega_n+\Delta\varepsilon)^2} + \frac{1-\cos(\omega_n-\Delta\varepsilon)t}{(\omega_n-\Delta\varepsilon)^2}\Big)\Big] \\ & + 2\kappa^2 \exp\Big[-2\kappa^2 \sum_n{}' C_n \Big(\frac{1-\cos(\omega_n+\Delta\varepsilon)t}{(\omega_n+\Delta\varepsilon)^2} + \frac{1-\cos(\omega_n-\Delta\varepsilon)t}{(\omega_n-\Delta\varepsilon)^2}\Big)\Big] \\ & \times \sum_n{}' C_n \int_0^t dt' \, \frac{\sin(\omega_n+\Delta\varepsilon)t'}{\omega_n+\Delta\varepsilon} \exp\Big[2\kappa^2 \sum_n{}' C_n \Big(\frac{1-\cos(\omega_n+\Delta\varepsilon)t'}{(\omega_n+\Delta\varepsilon)^2} + \frac{1-\cos(\omega_n-\Delta\varepsilon)t'}{(\omega_n-\Delta\varepsilon)^2}\Big)\Big]. \quad (53)\end{aligned}$$

The solution Eq. (53) has a part dependent on the initial value of $\langle 10|\rho_s(t)|10\rangle$ and a part independent of that.

To understand decoherence and the decay of the excited state ($|10\rangle$), we define two quantities: the coherence factor $\mathrm{C(t)} = \frac{|\langle 10|\rho_s(t)|01\rangle|}{|\langle 10|\rho_s(0)|01\rangle|}$ and the population of the excited state $\mathrm{P(t)} = \langle 10|\rho_s(t)|10\rangle$. We numerically solve the coupled differential equations given by Eq. (51) and its complex-conjugate equation and plot the dynamical behavior of C(t) in Figs. 3, 5(a), and 7. We also depict the time dependence of P(t) in Figs. 4, 5(b), and 8. We analyze below Figs. 3–8 and show that the period of oscillation and the amplitude of oscillation of both C(t) and P(t) increase as the site energy difference $\Delta\varepsilon$ approaches a harmonic ω_n; also, the closer the $\Delta\varepsilon$ is to ω_n, the smaller are the equilibrium values of C(t) and P(t). Furthermore, the closer ω_n is to $2g^2\omega$ (i.e., twice the polaronic energy), the more prominent are the period and amplitude of oscillations. Interestingly too, we find that the stronger the coupling g, the weaker is the decoherence and the decay of the excited state population.

In Figs. 3 and 4, we study three cases of proximity of $\Delta\varepsilon$ to ω_n: $\frac{\Delta\varepsilon}{\omega} = 2.5,\ 7.5,\ \&\ 14.5$; $\frac{\Delta\varepsilon}{\omega} = 2.9,\ 7.9,\ \&\ 14.9$; and $\frac{\Delta\varepsilon}{\omega} = 3.0,\ 8.0,\ \&\ 15.0$. One can see from Eq. (51) that, for values of $\Delta\varepsilon$ close to ω_n (i.e., for $\frac{\Delta\varepsilon}{\omega} = 2.9,\ 7.9,\ \&\ 14.9$), the dominant terms have arguments of the periodic functions being given by $(\omega_n - \Delta\varepsilon)t = 0.1\omega t$; consequently, there is a large period of oscillation (given by $\omega t = 20\pi$) in Fig. 3(b). Also, the amplitude of oscillation is dominated by the term $\sin[(\omega_n-\Delta\varepsilon)t]/(\omega_n-\Delta\varepsilon)$ and hence the amplitude increases with decreasing values of $(\omega_n - \Delta\varepsilon)$. Furthermore, the coherence factor also depends on the number of degenerate phonon states with eigenenergy ω_n; the contribution of this degeneracy [as seen from Eq. (51)] is determined by the term

$$\mathbb{C}^{\mathbb{N}} = \frac{\kappa^2}{\omega^2} \sum_{n_1,n_2;(n_1+n_2)=\mathbb{N}} C_n = \frac{\kappa^2}{\omega^2} \frac{(2g^2)^{\mathbb{N}}}{\mathbb{N}!}, \quad (54)$$

where $\sum_{n_1,n_2;(n_1+n_2)=\mathbb{N}}$ adds up all C_n with $(n_1+n_2) = \mathbb{N}$. The closeness of $\Delta\varepsilon$ to ω_n and the value of $\mathbb{C}^{\mathbb{N}}$ together determine the strength of decoherence. The value of $\mathbb{C}^{\mathbb{N}}$ increases with increasing $\mathbb{N} = n_1+n_2$ up to some limit as depicted in Fig. 1. One can also see that the maximum of $\mathbb{C}^{\mathbb{N}}$ occurs at phonon eigenenergy ω_n close to $2g^2\omega$. In other words, for a particular g, when $\Delta\varepsilon$ is close to twice the polaronic energy $g^2\omega$, decoherence is maximum with ω_n closest to $2g^2\omega$ making the dominant contribution. In second-order perturbation picture, the relevant process involves the particle hopping from one site to another and coming back to the initial site. Now, the initial state is described by the occupied site with polaronic energy (lattice distortion potential) $-g^2\omega$; whereas the intermediate state for perturbation theory corresponds to the occupied second-site being without distortion and the unoccupied first-site having distortion energy $+g^2\omega$ [see Fig. 2 given above and Fig. 2(a) in Ref. 18]. As the energy difference between the initial and the intermediate states [i.e., $(\varepsilon_1 - g^2\omega) - (\varepsilon_2 + g^2\omega) = \Delta\varepsilon - 2g^2\omega$] approaches zero, the hopping process becomes more dominant leading to stronger decoherence. The above observations that the period of oscillation being inversely proportional to $\Delta\varepsilon - \omega_n$ and that the values of $1/(\Delta\varepsilon - \omega_n)$ and $\mathbb{C}^{\mathbb{N}}$ together determine the strength of decoherence are also exemplified for the cases when $\Delta\varepsilon = \omega_n$ [through Fig. 3(c)

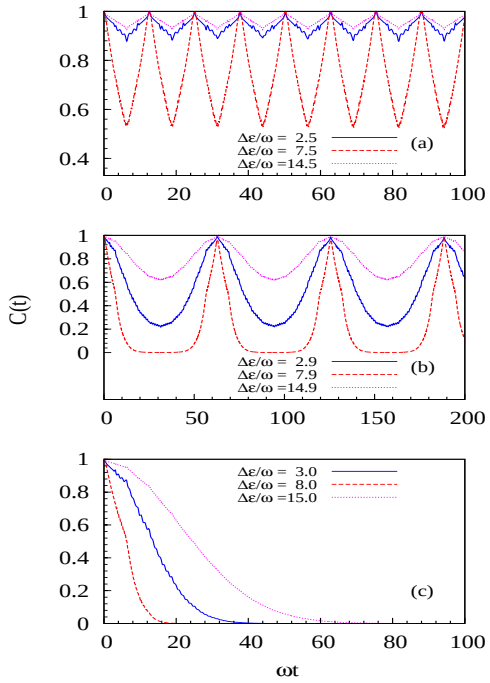

FIG. 3. Time dependence of C(t) for $\frac{J_\perp}{\omega} = 1.0$, $g = 2.0$, and when (a) $\frac{\Delta\varepsilon}{\omega} = 2.5, 7.5$ and 14.5; (b) $\frac{\Delta\varepsilon}{\omega} = 2.9, 7.9$ and 14.9; and (c) $\frac{\Delta\varepsilon}{\omega} = 3.0, 8.0$ and 15.0 .

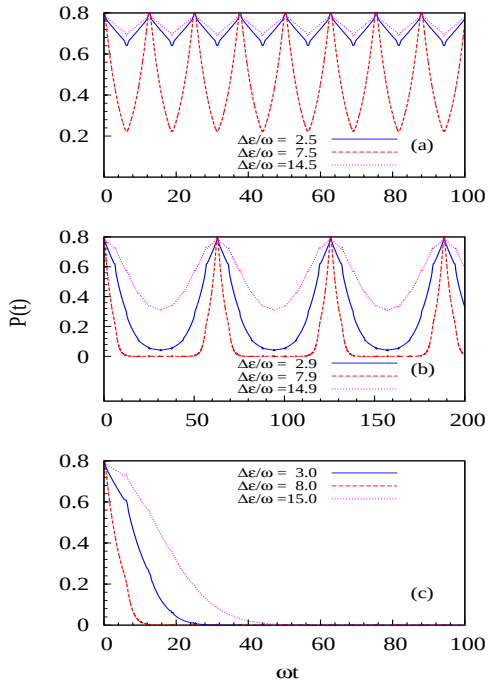

FIG. 4. Time dependence of P(t) for $\frac{J_\perp}{\omega} = 1.0$, P(0) = 0.8, $g = 2.0$, and when (a) $\frac{\Delta\varepsilon}{\omega} = 2.5, 7.5$ and 14.5; (b) $\frac{\Delta\varepsilon}{\omega} = 2.9, 7.9$ and 14.9; and (c) $\frac{\Delta\varepsilon}{\omega} = 3.0, 8.0$ and 15.0.

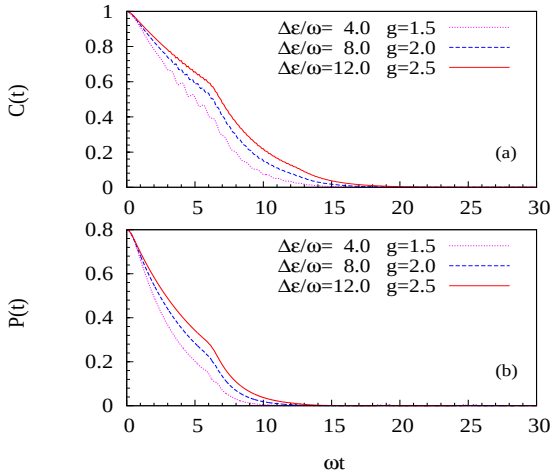

FIG. 5. Time dependence of (a) C(t) and (b) P(t) [with P(0) = 0.8] for different values of coupling g and $\frac{J_\perp}{\omega} = 1.0$ when $\Delta\varepsilon/\omega$ takes integer values closest to $2g^2$.

when $\frac{\Delta\varepsilon}{\omega} = 3.0,\ 8.0,\ \&\ 15.0]$ and when $|\Delta\varepsilon - \omega_n| = \omega/2$ [through Fig. 3(a) when $\frac{\Delta\varepsilon}{\omega} = 2.5,\ 7.5,\ \&\ 14.5]$. In Fig. 3(c) [3(a)], the period of oscillation is infinity $[4\pi/\omega]$ and the decoherence is stronger [weaker] than in Fig. 3(b). It should be clear that recoherence occurs in Fig. 3 because we are dealing with single mode phonons; the closer that $\Delta\varepsilon$ approaches ω_n, the later does the recoherence occur (i.e., recoherence time is inversely proportional to $\Delta\varepsilon - \omega_n$.).

Similar to the above analysis of Eq. (51), one can analyze Eq. (53) to gain an understanding of P(t). For comparatively large initial values $\langle 10|\rho_s(0)|10\rangle$, the time dependence of $\langle 10|\rho_s(t)|10\rangle$ is mainly determined by the homogeneous part in Eq. (53). The role of the inhomogeneous term can be understood from Fig. 6 by taking P(0) = 0 in Eq. (53). One can see a very small variation of the excited state population and the peak values of oscillations in Fig. 6 are comparable to the order of $\frac{|\kappa|}{|\Delta\varepsilon|}$ [i.e., $\sim O(10^{-2})$]; we have neglected $\frac{|\kappa|}{|\Delta\varepsilon|}$ compared to 1 in our calculations. So [when P(0) = 0], we can say that the system stays in the ground state for all practical purposes. Next, in Eq. (53), we see that the homogeneous part is dominated by the oscillatory terms with period of oscillation being inversely proportional to $\Delta\varepsilon - \omega_n$; here too the values of $1/(\Delta\varepsilon - \omega_n)$ and $\mathbb{C}^{\mathbb{N}}$ together determine the strength of decay of P(t) as can be seen from Figs. 4 (a), (b), and (c).

To understand the dependence of C(t) and P(t) on the strength of coupling, we study the variation of $\mathbb{C}^{\mathbb{N}}$ on g in Fig. 1. The peak value of $\mathbb{C}^{\mathbb{N}}$ decreases with increasing g, i.e., the maximum decoherence/decay (which occurs when $\Delta\varepsilon = 2g^2\omega$) decreases as the coupling becomes stronger. In Figs. 5(a) and (b), respectively, C(t) and P(t) are plotted for different values of g with $\frac{\Delta\varepsilon}{\omega}$ taking integer values closest to $2g^2$.

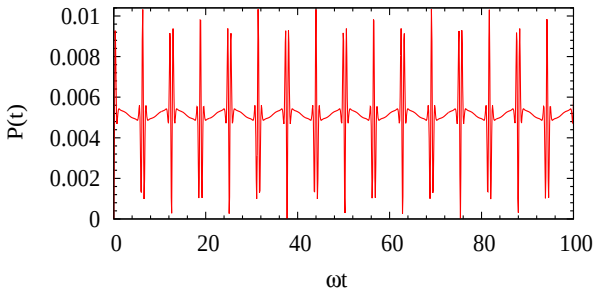

FIG. 6. Time dependence of P(t) for $\frac{\Delta\varepsilon}{\omega} = 2.5$ when $\frac{J_\perp}{\omega} = 1.0$, P(0) = 0, and $g = 2.0$.

Now, we like to determine the values of C(t) and P(t) at long times, i.e., at times much larger than the largest timescale in the process $\hbar/J_\perp e^{-g^2}$. To this end, in Eqs. (51) and (52), we multiply the oscillatory terms with a decay term $e^{-\eta t}$ (where $\eta \to 0^+$) and rewrite the equations as

$$\frac{d\langle 10|\tilde{\rho}_s(t)|01\rangle}{dt} = -i\kappa^2 {\sum_n}' C_n \Big[\langle 10|\tilde{\rho}_s(t)|01\rangle \Big(\frac{e^{-i(\omega_n-\Delta\varepsilon-i\eta)t}}{\omega_n-\Delta\varepsilon} - \frac{e^{i(\omega_n+\Delta\varepsilon+i\eta)t}}{\omega_n+\Delta\varepsilon} - \frac{2\Delta\varepsilon}{\omega_n^2-\Delta\varepsilon^2}\Big)$$
$$+ \langle 01|\tilde{\rho}_s(t)|10\rangle(-1)^{n_1+n_2} e^{i(2\Delta\varepsilon+i\eta)t}\Big(\frac{e^{i(\omega_n-\Delta\varepsilon)t}}{\omega_n-\Delta\varepsilon} - \frac{e^{-i(\omega_n+\Delta\varepsilon)t}}{\omega_n+\Delta\varepsilon} - \frac{2\Delta\varepsilon}{\omega_n^2-\Delta\varepsilon^2}\Big)\Big], \quad (55)$$

and

$$\frac{d\langle 10|\tilde{\rho}_s(t)|10\rangle}{dt} = -2\kappa^2 {\sum_n}' C_n e^{-\eta t}\Big[\langle 10|\tilde{\rho}_s(t)|10\rangle\Big(\frac{\sin(\omega_n+\Delta\varepsilon)t}{\omega_n+\Delta\varepsilon} + \frac{\sin(\omega_n-\Delta\varepsilon)t}{\omega_n-\Delta\varepsilon}\Big) - \frac{\sin(\omega_n+\Delta\varepsilon)t}{\omega_n+\Delta\varepsilon}\Big]. \quad (56)$$

We plot C(t) and P(t) in Figs. 7 and 8, respectively, for values of $\eta/\omega = 0.01$ and 0.02. For both the values of η, C(t) [as well as P(t)] attain the same equilibrium value. Here we should mention that, (for the chosen values of $\eta/\omega = 0.01$ and 0.02) although the decay term $e^{-\eta t}$ does diminish over the period of oscillation of C(t) and P(t), we got the same equilibrium values for much smaller values of η as well.

Lastly, we would like to compare the case of nonzero $\Delta\varepsilon$ with the case of $\Delta\varepsilon = 0$ using the plots in Figs. 9 and 10. To analyze decoherence using C(t) and decay of P(t), for each case, we use the corresponding eigenstate basis, i.e., $\{|10\rangle, |01\rangle\}$ for $\Delta\varepsilon \neq 0$ and $\Big\{\frac{|10\rangle-|01\rangle}{\sqrt{2}}, \frac{|10\rangle+|01\rangle}{\sqrt{2}}\Big\}$ for $\Delta\varepsilon = 0$; we note that $\frac{|10\rangle-|01\rangle}{\sqrt{2}}$ is the excited state for the case of $\Delta\varepsilon = 0$. We see that the periodicity of the cases with nonzero site energy [depicted in Figs. 3, 4, 9(a) and 10(a)] is determined by the closeness of $\Delta\varepsilon$ to

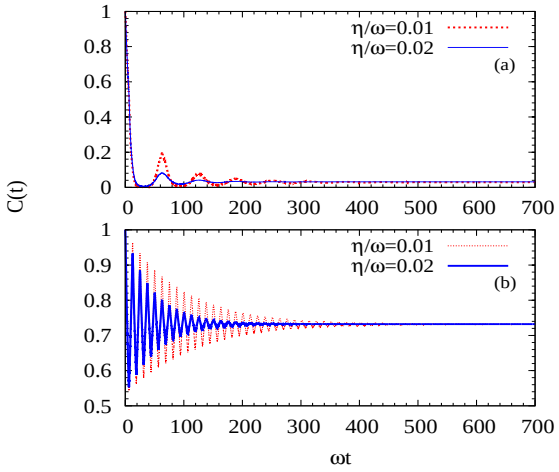

FIG. 7. Time dependence of C(t) for $\frac{J_\perp}{\omega} = 1.0$, $g = 2.0$, and when (a) $\frac{\Delta\varepsilon}{\omega} = 7.9$ and (b) $\frac{\Delta\varepsilon}{\omega} = 7.5$.

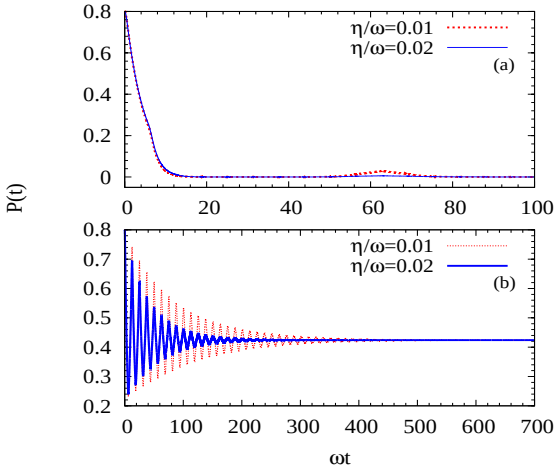

FIG. 8. Time dependence of P(t) for $\frac{J_\perp}{\omega} = 1.0$, P(0) = 0.8, $g = 2.0$, and when (a) $\frac{\Delta\varepsilon}{\omega} = 7.9$ and (b) $\frac{\Delta\varepsilon}{\omega} = 7.5$.

$\Delta\varepsilon/\omega = 0$			$\Delta\varepsilon/\omega = 2.5$		
g	C(t → ∞)	P(t → ∞)	g	C(t → ∞)	P(t → ∞)
1.5	0.970	0.794	1.5	0.916	0.683
2.0	0.993	0.799	2.0	0.984	0.778

TABLE I. Equilibrium values of C(t) and P(t) [with P(0) = 0.8] for $J_\perp/\omega = 0.5$ and various values of g when $\Delta\varepsilon/\omega = 0$ & 2.5.

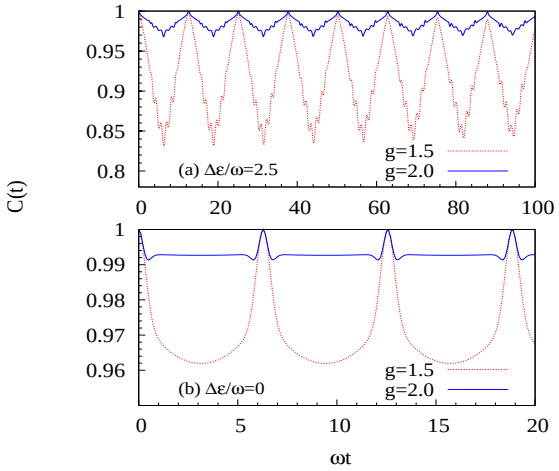

FIG. 9. Time dependence of C(t) for $\frac{J_\perp}{\omega} = 0.5$, $g = 1.5$ & 2.0, and when (a) $\frac{\Delta\varepsilon}{\omega} = 2.5$ and (b) $\frac{\Delta\varepsilon}{\omega} = 0$.

ω_n whereas the periodicity of the case with $\Delta\varepsilon = 0$ is determined by ω. For the case of $\Delta\varepsilon = 0$, in the strong coupling regime, since the system excitation energy $J_\perp e^{-g^2}$ is much smaller than ω, there is no possibility of energy exchange between the system and phonons. This results in smaller equilibrium values of C(t) and P(t) for the case with finite $\Delta\varepsilon$ compared to the case with $\Delta\varepsilon = 0$ as shown in Table I. Also, the oscillations of C(t) and P(t) are smaller for the case $\Delta\varepsilon = 0$ compared to the case of finite $\Delta\varepsilon$ as can be seen by comparing Figs. 9(b) and 10(b) with Figs. 9(a) and 10(a); here we chose $\Delta\varepsilon/\omega = 2.5$ so that $\Delta\varepsilon$ is far away from the nearest eigenenergies $\omega_n = 2\omega$ & 3ω. Furthermore, in Fig. 9(b) [Fig.10(b)] the ωt regions between two consecutive integer multiples of 2π [π] become flatter as the coupling g increases; as g increases, more number of excited states for phonons (with energy ω_n) contribute and produce destructive interference of phases resulting in the flat region (see Ref. 12 for details) [39]. On the other hand, in Figs. 9(a) and 10(a), only those states with ω_n close to $\Delta\varepsilon$ have a dominant contribution.

B. Multimode case

Here we deal with a more realistic case, i.e., we consider a continuous distribution of phonon frequencies and, for simplicity, allow a small window characterized by upper and lower limits. The generalized Hamiltonian for multimode phonons in the polaronic frame of reference is written as

$$H = \varepsilon_1(n_1 - \frac{1}{2}) + \varepsilon_2(n_2 - \frac{1}{2}) - \frac{J_\perp}{2}(b_1^\dagger b_2 + b_2^\dagger b_1) + J_\parallel(n_1 - \frac{1}{2})(n_2 - \frac{1}{2}) + \sum_{i,k}\omega_k a_{i,k}^\dagger a_{i,k} + \frac{1}{\sqrt{N}}\sum_{i,k} g_k\omega_k(n_i - \frac{1}{2})(a_{i,k} + a_{i,k}^\dagger), \quad (57)$$

where $a_{i,k}$ destroys a phonon with momentum k at site i and N is the number of phonon modes. To perform perturbation theory with ease, we perform Lang-Firsov transformation $H^L = e^S H e^{-S} = H_s^L + H_{env}^L + H_I^L$ where $S = -\frac{1}{\sqrt{N}}\sum_{i,k} g_k(n_i - \frac{1}{2})(a_{i,k} - a_{i,k}^\dagger)$. Then, the components of H^L (i.e., the systems part H_s^L, the environment part H_{env}^L, and the interaction part H_I^L) are expressed as

$$H_s^L = \varepsilon_1(n_1 - \frac{1}{2}) + \varepsilon_2(n_2 - \frac{1}{2}) + J_\parallel(n_1 - \frac{1}{2})(n_2 - \frac{1}{2}) - \frac{J_\perp e^{-\frac{1}{N}\sum_k g_k^2}}{2}(b_1^\dagger b_2 + b_2^\dagger b_1), \quad (58)$$

$$H_{env}^L = \sum_{i,k}\omega_k a_{i,k}^\dagger a_{i,k}, \quad (59)$$

and

$$H_I^L = -\frac{1}{2}[J_\perp^+ b_1^\dagger b_2 + J_\perp^- b_2^\dagger b_1], \quad (60)$$

where

$$J_\perp^\pm = J_\perp e^{\pm\frac{1}{\sqrt{N}}\sum_k\ g_k[(a_{2,k} - a_{2,k}^\dagger) - (a_{1,k} - a_{1,k}^\dagger)]} - J_\perp e^{-\frac{1}{N}\sum_k g_k^2}. \quad (61)$$

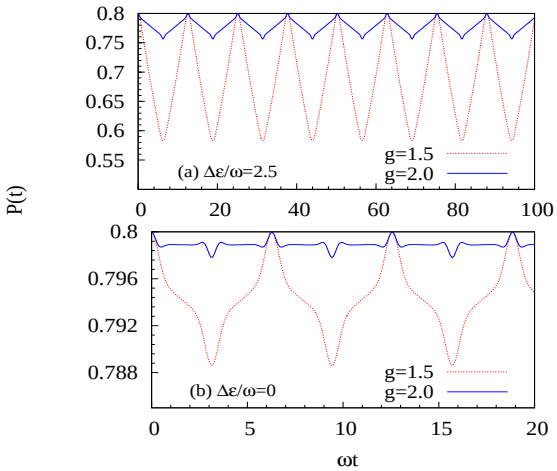

FIG. 10. Time dependence of P(t) for $\frac{J_\perp}{\omega} = 0.5$, P(0) = 0.8, $g = 1.5$ & 2.0, and when (a) $\frac{\Delta\varepsilon}{\omega} = 2.5$ and (b) $\frac{\Delta\varepsilon}{\omega} = 0$.

Now, we use the non-Markovian master Eq. (47) to study the dynamics of the reduced density matrix. We calculate below the matrix element ${}_{ph}\langle\{0_1^k\},\{0_2^k\}|H_I^L|\{m_1^k\},\{m_2^k\}\rangle_{ph}$ with m_1^k and m_2^k being the occupation numbers of the k-th mode phonons at site 1 and site 2, respectively.

$$\begin{aligned}&{}_{ph}\langle\{0_1^k\},\{0_2^k\}|H_I^L|\{m_1^k\},\{m_2^k\}\rangle_{ph}\\ &=-\frac{J_\perp}{2}e^{-\frac{1}{N}\sum_k g_k^2}\left(\prod_k\frac{(\frac{g_k}{\sqrt{N}})^{(m_1^k+m_2^k)}}{\sqrt{m_1^k!m_2^k!}}\right)\\ &\times(-1)^{\sum_k m_1^k}\left[b_1^\dagger b_2+(-1)^{\sum_k(m_1^k-m_2^k)}b_2^\dagger b_1\right].\end{aligned}\tag{62}$$

Using the above result and Eqs. (48) and (49) $\Big[$with κ replaced by $\bar{\kappa}\equiv-\frac{J_\perp e^{-\frac{1}{N}\sum_k g_k^2}}{2}$ $\Big]$, we calculate the four terms in the master Eq. (47); in the regime where $\Delta\varepsilon\gg J_\perp e^{-\frac{1}{N}\sum_k g_k^2}$, we can write the differential equation for $\langle 10|\tilde{\rho}_s(t)|01\rangle$ to be

$$\begin{aligned}\frac{d\langle 10|\tilde{\rho}_s(t)|01\rangle}{dt}=-\bar{\kappa}^2\sum_{\{n_1^k\},\{n_2^k\}}{}'\bar{C}_n\int_0^t d\tau\Bigg[&\langle 10|\tilde{\rho}_s(t)|01\rangle\left(e^{i(\bar{\omega}_n+\Delta\varepsilon)T}+e^{-i(\bar{\omega}_n-\Delta\varepsilon)T}\right)\\&-\langle 01|\tilde{\rho}_s(t)|10\rangle(-1)^{\sum_k(n_1^k-n_2^k)}e^{2i\Delta\varepsilon t}\left(e^{i(\bar{\omega}_n-\Delta\varepsilon)T}+e^{-i(\bar{\omega}_n+\Delta\varepsilon)T}\right)\Bigg].\end{aligned}\tag{63}$$

The corresponding complex conjugate equation would describe the dynamics for $\langle 01|\tilde{\rho}_s(t)|10\rangle$. Here, we have defined $\bar{\omega}_n\equiv\sum_k\omega_k(n_1^k+n_2^k)$, $\bar{C}_n\equiv\prod_k\frac{(\frac{g_k}{\sqrt{N}})^{2(n_1^k+n_2^k)}}{n_1^k!n_2^k!}$, $T\equiv t-\tau$, and $\sum'_{\{n_1^k\},\{n_2^k\}}$ as the sum over all combinations of $\{n_1^k\}$ and $\{n_2^k\}$ excluding the case when $\{n_1^k\}=\{0_1^k\}$ and $\{n_2^k\}=\{0_2^k\}$. Similarly, one can obtain the following differential equation for $\langle 10|\tilde{\rho}_s(t)|10\rangle$:

$$\begin{aligned}\frac{d\langle 10|\tilde{\rho}_s(t)|10\rangle}{dt}=-\bar{\kappa}^2\sum_{\{n_1^k\},\{n_2^k\}}{}'\bar{C}_n\int_0^t d\tau\Bigg[&2\langle 10|\tilde{\rho}_s(t)|10\rangle\cos(\Delta\varepsilon T)\left(e^{i\bar{\omega}_nT}+e^{-i\bar{\omega}_nT}\right)\\&-\left(e^{i(\bar{\omega}_n+\Delta\varepsilon)T}+e^{-i(\bar{\omega}_n+\Delta\varepsilon)T}\right)\Bigg].\end{aligned}\tag{64}$$

Now, to get a closed form of the coefficients in Eqs. (63) and (64), we write

$$\begin{aligned}\sum_{\{n_1^k\},\{n_2^k\}}{}'\bar{C}_ne^{\pm i\bar{\omega}_nT}&=\prod_k\left(\sum_{n_1^k}\frac{\left(\frac{g_k^2}{N}\right)^{n_1^k}}{n_1^k!}e^{\pm i\omega_kn_1^kT}\sum_{n_2^k}\frac{\left(\frac{g_k^2}{N}\right)^{n_2^k}}{n_2^k!}e^{\pm i\omega_kn_2^kT}\right)-1\\&=\exp\left[\sum_k2\frac{g_k^2}{N}e^{\pm i\omega_kT}\right]-1\\&=\exp\left[\frac{2}{N\pi}\int_0^\infty d\omega\frac{J(\omega)}{\omega^2}e^{\pm i\omega T}\right]-1,\end{aligned}\tag{65}$$

where the spectral function of the phonon bath $J(\omega)=\pi\sum_k g_k^2\omega_k^2\delta(\omega-\omega_k)$ characterizes the HCB-phonon coupling for different phonon-frequency modes. Using the above expression, we can write the differential Eqs. (63) and (64) as

$$\begin{aligned}&\frac{d\langle 10|\tilde{\rho}_s(t)|01\rangle}{dt}\\&=-2\bar{\kappa}^2\int_0^t d\tau\Bigg[\langle 10|\tilde{\rho}_s(t)|01\rangle e^{i\Delta\varepsilon T}\left(\exp\Big[\frac{2}{N\pi}\int_0^\infty d\omega\frac{J(\omega)}{\omega^2}\cos(\omega T)\Big]\cos\Big[\frac{2}{N\pi}\int_0^\infty d\omega\frac{J(\omega)}{\omega^2}\sin(\omega T)\Big]-1\right)\\&\quad-\langle 01|\tilde{\rho}_s(t)|10\rangle e^{i\Delta\varepsilon(t+\tau)}\left(\exp\Big[-\frac{2}{N\pi}\int_0^\infty d\omega\frac{J(\omega)}{\omega^2}\cos(\omega T)\Big]\cos\Big[\frac{2}{N\pi}\int_0^\infty d\omega\frac{J(\omega)}{\omega^2}\sin(\omega T)\Big]-1\right)\Bigg],\end{aligned}\tag{66}$$

and

$$\frac{d\langle 10|\tilde{\rho}_s(t)|10\rangle}{dt} = -2\bar{\kappa}^2\int_0^t d\tau\Bigg[2\langle 10|\tilde{\rho}_s(t)|10\rangle\cos(\Delta\varepsilon T)\Bigg(\exp\Big[\frac{2}{N\pi}\int_0^\infty d\omega\frac{J(\omega)}{\omega^2}\cos(\omega T)\Big]\cos\Big[\frac{2}{N\pi}\int_0^\infty d\omega\frac{J(\omega)}{\omega^2}\sin(\omega T)\Big]-1\Bigg) - \Bigg(\exp\Big[\frac{2}{N\pi}\int_0^\infty d\omega\frac{J(\omega)}{\omega^2}\cos(\omega T)\Big]\cos\Big[\Delta\varepsilon T+\frac{2}{N\pi}\int_0^\infty d\omega\frac{J(\omega)}{\omega^2}\sin(\omega T)\Big]-\cos(\Delta\varepsilon T)\Bigg)\Bigg]. \quad (67)$$

The differential Eq. (67) can be solved analytically and the solution is written as

$$\langle 10|\rho_s(t)|10\rangle = e^{-\int_0^t dt' A(t')}\Bigg(\langle 10|\rho_s(0)|10\rangle + \int_0^t dt' B(t') e^{\int_0^{t'} dt'' A(t'')}\Bigg), \quad (68)$$

where

$$A(t) = 4\bar{\kappa}^2\int_0^t d\tau\,\cos(\Delta\varepsilon T)\Bigg(\exp\Big[\frac{2}{N\pi}\int_0^\infty d\omega\frac{J(\omega)}{\omega^2}\cos(\omega T)\Big]\cos\Big[\frac{2}{N\pi}\int_0^\infty d\omega\frac{J(\omega)}{\omega^2}\sin(\omega T)\Big]-1\Bigg), \quad (69)$$

and

$$B(t) = 2\bar{\kappa}^2\int_0^t d\tau\Bigg(\exp\Big[\frac{2}{N\pi}\int_0^\infty d\omega\frac{J(\omega)}{\omega^2}\cos(\omega T)\Big]\cos\Big[\Delta\varepsilon T+\frac{2}{N\pi}\int_0^\infty d\omega\frac{J(\omega)}{\omega^2}\sin(\omega T)\Big]-\cos(\Delta\varepsilon T)\Bigg). \quad (70)$$

In principle, $J(\omega)$ can assume a variety of forms based on the nature of the phonon bath; however, for simplicity, we use a continuous uniform distribution of phonon frequencies within a small frequency window characterized by an upper cutoff ω_u and a lower cutoff ω_l. The density of states for Einstein phonons is described by $\mathrm{D}(\omega_k) = N\delta(\omega_k - \omega_0)$ where ω_0 is a fixed frequency and N is the number of phonon modes. Moreover, we consider a weak k-dependence of the coupling strength g_k and write

$$\mathrm{D}(\omega_k)g_k^2 = N\delta(\omega_k-\omega_0)g^2. \quad (71)$$

Here we should mention that in systems such as the manganites (where the carriers are coupled predominantly only to optical phonons), the weak k-dependence of g_k is quite valid. Following Eq. (71) we make a simple generalization of Einstein model and replace the Dirac delta function by a box function of width $(\omega_u-\omega_l)$ and height $\frac{1}{(\omega_u-\omega_l)}$

$$\mathrm{D}(\omega_k)g_k^2 = g^2\frac{N}{\omega_u-\omega_l}\Theta(\omega_k-\omega_l)\Theta(\omega_u-\omega_k), \quad (72)$$

where $\Theta(\omega)$ is the unit step function. With the above form for the density of states, we calculate the following:

$$\begin{aligned}\frac{1}{N\pi}\int_0^\infty\frac{J(\omega)}{\omega^2}d\omega &= \frac{1}{N}\sum_k g_k^2\\ &= \frac{1}{N}\int_0^\infty d\omega_k\mathrm{D}(\omega_k)g_k^2\\ &= \int_{\omega_l}^{\omega_u} d\omega_k\frac{g^2}{\omega_u-\omega_l}\\ &= g^2, \end{aligned} \quad (73)$$

$$\begin{aligned}\frac{1}{N\pi}\int_0^\infty\frac{J(\omega)}{\omega^2}\cos\omega T d\omega &= \frac{1}{N}\sum_k g_k^2\cos\omega_k T\\ &= \frac{1}{N}\int_0^\infty d\omega_k\mathrm{D}(\omega_k)g_k^2\cos\omega_k T\\ &= \frac{g^2}{(\omega_u-\omega_l)T}(\sin\omega_u T-\sin\omega_l T)\\ &= \frac{2g^2}{(\omega_u-\omega_l)T}\cos\Big[\frac{(\omega_u+\omega_l)T}{2}\Big]\\ &\quad\times\sin\Big[\frac{(\omega_u-\omega_l)T}{2}\Big], \end{aligned} \quad (74)$$

and

$$\frac{1}{N\pi}\int_0^\infty \frac{J(\omega)}{\omega^2}\sin\omega T d\omega = \frac{1}{N}\sum_k g_k^2 \sin\omega_k T$$
$$= \frac{1}{N}\int_0^\infty d\omega_k \mathrm{D}(\omega_k) g_k^2 \sin\omega_k T$$
$$= \frac{g^2}{(\omega_u-\omega_l)T}(\cos\omega_l T - \cos\omega_u T)$$
$$= \frac{2g^2}{(\omega_u-\omega_l)T}\sin\Big[\frac{(\omega_u+\omega_l)T}{2}\Big] \times \sin\Big[\frac{(\omega_u-\omega_l)T}{2}\Big]. \quad (75)$$

Using the above integrals, we solve the differential Eq. (66) numerically and plot the coherence factor C(t) in Fig. (11). Here, unlike the single-mode case, we have a continuum of phonon frequencies due to which the various harmonics in Eq. (63) do not all rephase at the same time leading to destructive interference, i.e., an irreversible decay of C(t).

To explain the periodicity of the plot in Fig. 11, we rewrite Eq. (63) as

$$\frac{d\langle 10|\tilde{\rho}_s(t)|01\rangle}{dt} = -i\bar{\kappa}^2 \sum_{\{n_1^k\},\{n_2^k\}}{}' \bar{C}_n \Bigg[\langle 10|\tilde{\rho}_s(t)|01\rangle\Big(\frac{e^{-i(\bar{\omega}_n-\Delta\varepsilon)t}}{\bar{\omega}_n-\Delta\varepsilon} - \frac{e^{i(\bar{\omega}_n+\Delta\varepsilon)t}}{\bar{\omega}_n+\Delta\varepsilon} - \frac{2\Delta\varepsilon}{\bar{\omega}_n^2-\Delta\varepsilon^2}\Big)$$
$$+ \langle 01|\tilde{\rho}_s(t)|10\rangle(-1)^{\sum_k (n_1^k-n_2^k)} e^{2i\Delta\varepsilon t}\Big(\frac{e^{i(\bar{\omega}_n-\Delta\varepsilon)t}}{\bar{\omega}_n-\Delta\varepsilon} - \frac{e^{-i(\bar{\omega}_n+\Delta\varepsilon)t}}{\bar{\omega}_n+\Delta\varepsilon} - \frac{2\Delta\varepsilon}{\bar{\omega}_n^2-\Delta\varepsilon^2}\Big)\Bigg]. \quad (76)$$

It is of interest to note that the structures of Eqs. (51) and (76) are very similar; hence the explanations that were offered in the single-mode case, for the period and amplitude of oscillations as well as for the equilibrium values of C(t), hold also for the multimode case. For the circumstance in Fig. 11 (b), the contribution from the phonon state ω_u dominates because it is the frequency that is closest to $\Delta\varepsilon$ and $\Delta\varepsilon - \omega_u$ ($<< \omega_u$) is comparable to the width of the allowed-frequency window $\omega_u - \omega_l$. Then, the period of oscillation in Eq. (76) can be obtained approximately from the case $|(\bar{\omega}_n - \Delta\varepsilon)t| = |(\omega_u - \Delta\varepsilon)t| = 0.1\omega_u t$; thus the period is approximately $20\pi/\omega_u$. Furthermore, since $\Delta\varepsilon$ is close to $\bar{\omega}_n$, only a few frequencies contribute to the destructive interference leading to a gradual decay of the amplitude of oscillation in Fig. 11 (b).

For the situation where $\Delta\varepsilon$ equals any of the phonon eigenenergies $\bar{\omega}_n$ [such as in Fig. 11 (c)], there is a complete decay of coherence due to strong exchange of energy. When $\Delta\varepsilon$ is away from $\bar{\omega}_n$ [which is the case in Fig. 11 (a)], there are a number of dominant phonon states having comparable contributions and these states interfere destructively resulting in a quick decay of amplitude.

Next, we study the population P(t) of the excited state $|10\rangle$ and depict its variation in Fig. 12. When the excited state is initially largely populated (such as in Fig. 12 where $\langle 10|\rho_s(0)|10\rangle = 0.8$), the behavior of P(t) is mainly dictated by the homogeneous part of the solution given in Eq. (64). To explain the behavior of Fig. 12, we rewrite Eq. (64) as follows:

$$\frac{d\langle 10|\tilde{\rho}_s(t)|10\rangle}{dt} = -2\bar{\kappa}^2 \sum_{\{n_1^k\},\{n_2^k\}}{}' \bar{C}_n \Bigg[\langle 10|\tilde{\rho}_s(t)|10\rangle\Big(\frac{\sin(\bar{\omega}_n+\Delta\varepsilon)t}{\bar{\omega}_n+\Delta\varepsilon} + \frac{\sin(\bar{\omega}_n-\Delta\varepsilon)t}{\bar{\omega}_n-\Delta\varepsilon}\Big) - \frac{\sin(\bar{\omega}_n+\Delta\varepsilon)t}{\bar{\omega}_n+\Delta\varepsilon}\Bigg]. \quad (77)$$

Since the structures of Eqs. (52) and (77) are very similar, we expect that the single-mode and multimode cases will have similar justifications for the period and

amplitude of oscillations as well as for the equilibrium values of P(t). The cases of $\Delta\varepsilon$ considered in Fig. 12 are the same as those studied in Fig. 11; furthermore, the same explanations hold for the period and decay of oscillations in these two figures.

Lastly, we elucidate through Fig. 13 the multi-mode cases $\left[\text{of } \Delta\varepsilon \text{ being an integer multiple of } \omega_{\rm avg} \equiv \frac{1}{N}\sum_k \omega_k = (\omega_u + \omega_l)/2\right]$ when the coherence C(t) and the excited state population P(t) undergo complete decay. Similar to the single-mode case [depicted in Figs. 3(c) and 4(c)], here too the maximum decay of both C(t) and P(t) occurs when $\Delta\varepsilon$ is equal to twice the polaron energy $\frac{1}{N}\sum_k g_k^2\omega_k$ (i.e., $2g^2\omega_{\rm avg}$ for our density of states).

V. DISCUSSION AND CONCLUSIONS

In this work we considered two models of HCB, characterized by strong HCB-phonon coupling and antiadiabaticity, with the initial state involving no correlation between the system and the environment in the polaronic frame of reference (where the interaction term is weak). These two models are a generalization of the systems studied in Ref. 12. (i) We have shown that an infinite-range HCB model subject to Markovian dynamics does not show decoherence or decay of excited state population. It is the long-range nature of the Hamiltonian and the negligible renormalized hopping (compared to the phonon energy) that preserve the eigenstates of the system coupled to strong local optical phonons and ensure decoherence free dynamics. (ii) The more realistic case, of non-Markovian dynamics and site energy differences being non-negligible compared to phonon energy, has been analyzed for an amenable two-site system. When the site-energy difference is not close to a phonon eigenenergy, the amount of decoherence and decay of excited state are both quite small and close to the Markovian results; whereas, decoherence and decay be-

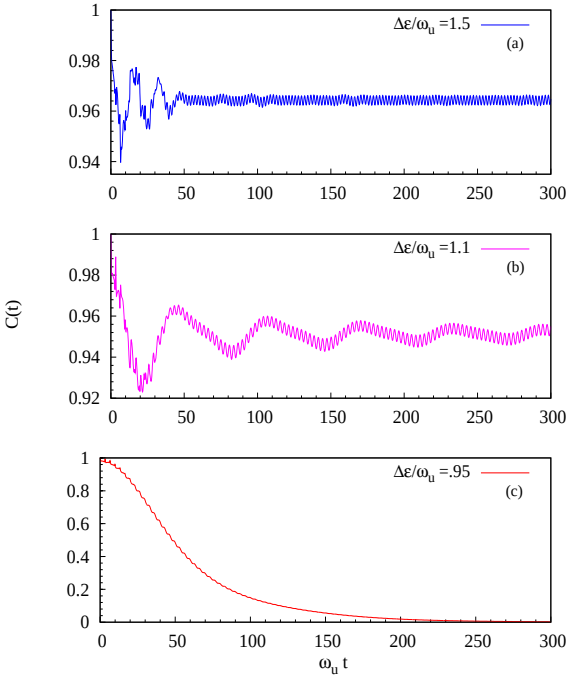

FIG. 11. Time dependence of C(t) for $\frac{J_\perp}{\omega_u} = 1.0$, $\frac{\omega_l}{\omega_u} = 0.9$, $g = 2.0$ and different values of $\frac{\Delta\varepsilon}{\omega_u}$ leading to different scenarios.

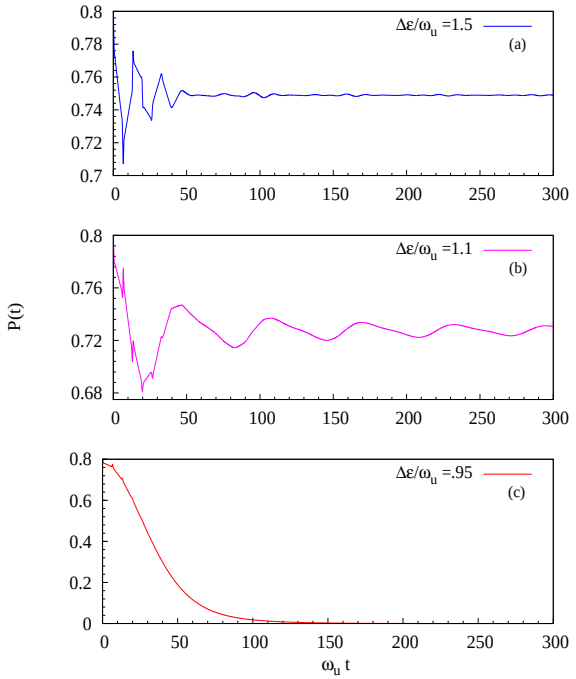

FIG. 12. Time dependence of P(t) for $\frac{J_\perp}{\omega_u} = 1.0$, P(0) = 0.8, $\frac{\omega_l}{\omega_u} = 0.9$, $g = 2.0$ and different values of $\frac{\Delta\varepsilon}{\omega_u}$.

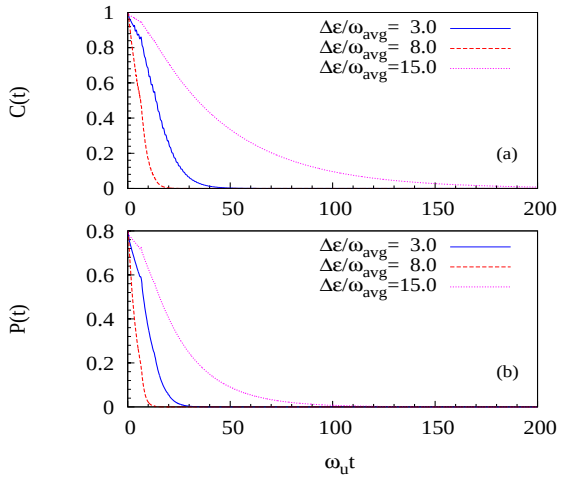

FIG. 13. Depiction of complete decay of (a) C(t) and (b) P(t) [with P(0) = 0.8] at different integer values of $\frac{\Delta\varepsilon}{\omega_{\rm avg}}$ when $\frac{J_\perp}{\omega_u} = 1.0$ and $g = 2.0$. The maximum decay occurs when $\Delta\varepsilon = 2g^2\omega_{\rm avg}$.

come prominent as system energy approaches a phonon eigenenergy.

We should mention that the approximate results obtained in the previous section (by neglecting $\frac{|\kappa|}{|\Delta\varepsilon|}$ compared to 1) are very close to the results obtained without any approximation (i.e., using the full expressions obtained in the appendix). Moreover, for the numerical results in the previous section, we used fourth-order Runge-Kutta for solving differential equations and Gaussian quadrature for numerical integrations.

We will now make a few general remarks regarding the range of hopping in a multi-site case. In contrast to our long-range model involving distance-independent hopping of HCBs, if we were to consider a chain with nearest-neighbor (NN) hopping $\Big[$of the type $\sum_i\{\frac{-J_\perp}{2}(b_i^\dagger b_{i+1}+$ H.c.$)+J_\parallel(n_i-\frac{1}{2})(n_{i+1}-\frac{1}{2})\}$ (with $J_\parallel=0$)$\Big]$ and strongly couple the HCBs to local phonons $\Big[$by introducing the additional terms $g\omega\sum_i(n_i-\frac{1}{2})(a_i^\dagger+a_i)+\omega\sum_i a_i^\dagger a_i\Big]$, we get decoherence for the case of half-filling. The NN-hopping system transits from a superfluid, with large values of the off-diagonal density matrix terms $\Big[$i.e., $< b_i^\dagger\sum_{j\neq i}b_j >=$ Bose-Einstein condensate occupation number $n_0\propto\sqrt{N}$ (see Ref. 19)$\Big]$, to a charge-density-wave state with significantly diminished off-diagonal density matrix terms $\Big(< b_i^\dagger\sum_{j\neq i}b_j >\Big)$. The above analysis can be mapped (through a HCB-to-spin transformation and then a Wigner-Jordan transformation) on to the analysis in Ref. 14 dealing with the transition from a Luttinger liquid to a charge-density-wave. Furthermore, the eigenstates of the effective Hamiltonian are not the same as the original NN-hopping model (for the $J_\parallel=0$ case); the effective Hamiltonian contains additional next-nearest-neighbor hopping terms $b_{i+1}^\dagger b_{i-1}$ and additional NN repulsion terms $n_{i+1}n_i$ that are not present in the original Hamiltonian [see Eqs. (4) and (5) in Ref. 14]. It is important to note that the infinite-range HCB model gives decoherence free behavior whereas the NN HCB model does not; thus, the range of interaction determines the decoherence of the system even when $J^\star e^{-g^2}\ll\omega$.

Although the analysis in this paper is valid for optical phonons, it can also accommodate acoustic phonons in small systems because the smallest wavevector, for a system with fixed boundaries, is inversely proportional to the system size; hence, for a small system $\Delta\varepsilon$ can be different from the eigenenergies of acoustic phonons. Furthermore, based on our study of a two-site system, our inferences can be extrapolated to a many-site situation, namely: as long as the various site-energy differences in a multi-site (as well as a many-body) case are away from the phonon eigenenergies, the decoherence will be small. This also implies that, to realize large coherence, the phonon density-of-states should vanish below a lower cut-off frequency. Lastly, the above analysis is valid in the regime $k_BT/\omega\ll 1$; the finite temperature case $k_BT/\omega\gtrsim 1$ needs additional extensive considerations and will be dealt with elsewhere.

The two-site case can be thought of as a system of an acceptor and a donor with different site energies (due to defects, impurities, etc.); the dynamics of population transfer between them as well as the two-site coherence are important for understanding many physical systems such as a double quantum dot (DQD) acting as a qubit for quantum computation [12], artificial light-harvesters, etc. An oxide- (i.e., manganite-) based DQD [12] can serve as a charge qubit and meet the demands of miniaturization as it has very small decoherence (compared to a semiconductor DQD) and its size can also be much smaller than a semiconductor DQD [10]. Additionally, understanding the high ($> 90\%$) quantum efficiency of energy transport between various chlorophyll molecules in photosynthesis is important to design artificial solar energy applications; minimizing the decoherence in an interacting many-spin system coupled to the environment is quite useful for developing quantum computer architecture. Our analysis of a many-body HCB model with Markovian dynamics is a step to meet the above ends.

VI. ACKNOWLEDGMENTS

One of the authors (S. Y.) would like to thank G. Baskaran, P. B. Littlewood, R. Simon, S. Ghosh, and S. Reja for valuable discussions.

Appendix A

Here, we calculate the four terms (on the right hand side) of the integrand in the following master equation obtained from Eq. (47) in the main text.

$$\begin{aligned}\frac{d\langle 10|\tilde{\rho}_s(t)|01\rangle}{dt}=-\sum_n\int_0^t d\tau\Big[\;&\langle 10|_{ph}\langle 0|\tilde{H}_I^L(t)|n\rangle_{ph}\;{}_{ph}\langle n|\tilde{H}_I^L(\tau)|0\rangle_{ph}\tilde{\rho}_s(t)|01\rangle\\&-\langle 10|\;{}_{ph}\langle n|\tilde{H}_I^L(t)|0\rangle_{ph}\tilde{\rho}_s(t)_{ph}\langle 0|\tilde{H}_I^L(\tau)|n\rangle_{ph}|01\rangle\\&-\langle 10|\;{}_{ph}\langle n|\tilde{H}_I^L(\tau)|0\rangle_{ph}\tilde{\rho}_s(t)_{ph}\langle 0|\tilde{H}_I^L(t)|n\rangle_{ph}|01\rangle\\&+\langle 10|\tilde{\rho}_s(t)_{ph}\langle 0|\tilde{H}_I^L(\tau)|n\rangle_{ph}\;{}_{ph}\langle n|\tilde{H}_I^L(t)|0\rangle_{ph}|01\rangle\Big].\end{aligned}\tag{A1}$$

The First term is evaluated as follows:

$$
\begin{aligned}
&\sum_n{}'\langle 10|_{ph}\langle 0|\tilde{H}_I^L(t)|n\rangle_{ph}\ {}_{ph}\langle n|\tilde{H}_I^L(\tau)|0\rangle_{ph}\tilde{\rho}_s(t)|01\rangle \\
&= \sum_n{}'\langle 10|e^{iH_s^L t}{}_{ph}\langle 0|H_I^L|n\rangle_{ph}e^{-iH_s^L(t-\tau)}{}_{ph}\langle n|H_I^L|0\rangle_{ph}e^{-iH_s^L\tau}\tilde{\rho}_s(t)|01\rangle e^{-i\omega_n(t-\tau)} \\
&= \kappa^2\sum_n{}' C_n\langle 10|e^{iH_s^L t}(b_1^\dagger b_2+(-1)^{(n_1+n_2)}b_2^\dagger b_1)e^{-iH_s^L(t-\tau)}\Big(b_2^\dagger b_1+(-1)^{n_1+n_2}b_1^\dagger b_2\Big)e^{-iH_s^L\tau}\tilde{\rho}_s(t)|01\rangle e^{-i\omega_n(t-\tau)} \\
&= \kappa^2\sum_n{}' C_n\Big[\langle 10|\tilde{\rho}_s(t)|01\rangle\Big\{p(t)p(t-\tau)p^*(\tau)+(-1)^{(n_1+n_2)}\kappa^2 q(t)q(t-\tau)p^*(\tau) \\
&\qquad\qquad +\kappa^2 q(t)p^*(t-\tau)q(\tau)-(-1)^{(n_1+n_2)}\kappa^2 p(t)q(t-\tau)q(\tau)\Big\} \\
&\qquad -i\kappa\langle 01|\tilde{\rho}_s(t)|01\rangle\Big\{p(t)p(t-\tau)q(\tau)+\kappa^2(-1)^{(n_1+n_2)}q(t)q(t-\tau)q(\tau) \\
&\qquad\qquad -q(t)p^*(t-\tau)p(\tau)+(-1)^{(n_1+n_2)}p(t)q(t-\tau)p(\tau)\Big\}\Big]e^{-i\omega_n(t-\tau)}\ . \qquad \text{(A2)}
\end{aligned}
$$

The second term is given by

$$
\begin{aligned}
&\sum_n{}'\langle 10|\ {}_{ph}\langle n|\tilde{H}_I^L(t)|0\rangle_{ph}\tilde{\rho}_s(t)_{ph}\langle 0|\tilde{H}_I^L(\tau)|n\rangle_{ph}|01\rangle \\
&= \sum_n{}'\langle 10|e^{iH_s^L t}{}_{ph}\langle n|H_I^L|0\rangle_{ph}e^{-iH_s^L t}\tilde{\rho}_s(t)e^{iH_s^L\tau}\langle 0|H_I^L|n\rangle_{ph}e^{-iH_s^L\tau}|01\rangle e^{i\omega_n(t-\tau)} \\
&= \kappa^2\sum_n{}' C_n\langle 10|e^{iH_s^L t}\Big(b_2^\dagger b_1+(-1)^{n_1+n_2}b_1^\dagger b_2\Big)e^{-iH_s^L t}\tilde{\rho}_s(t)e^{iH_s^L\tau}\Big(b_1^\dagger b_2+(-1)^{(n_1+n_2)}b_2^\dagger b_1\Big)e^{-iH_s^L\tau}|01\rangle e^{i\omega_n(t-\tau)} \\
&= \kappa^2\sum_n{}' C_n\Big[\kappa^2\langle 10|\tilde{\rho}_s(t)|01\rangle\Big\{(-1)^{(n_1+n_2)}q(t)q(\tau)p(t)p(\tau)-q(t)p^*(\tau)p(t)q(\tau) \\
&\qquad\qquad -p^*(t)q(\tau)q(t)p(\tau)+(-1)^{(n_1+n_2)}p^*(t)p^*(\tau)q(t)q(\tau)\Big\} \\
&\qquad +\langle 01|\tilde{\rho}_s(t)|10\rangle\Big\{(-1)^{(n_1+n_2)}p^2(t)p^2(\tau)+\kappa^2 p^2(t)q^2(\tau) \\
&\qquad\qquad +\kappa^2 q^2(t)p^2(\tau)+(-1)^{(n_1+n_2)}\kappa^4 q^2(t)q^2(\tau)\Big\} \\
&\qquad +i\kappa\langle 10|\tilde{\rho}_s(t)|10\rangle\Big\{-(-1)^{(n_1+n_2)}q(t)p^2(\tau)p(t)-\kappa^2 q(t)q^2(\tau)p(t) \\
&\qquad\qquad +p^*(t)p^2(\tau)q(t)+(-1)^{(n_1+n_2)}\kappa^2 p^*(t)q^2(\tau)q(t)\Big\} \\
&\qquad +i\kappa\langle 01|\tilde{\rho}_s(t)|01\rangle\Big\{(-1)^{(n_1+n_2)}p^2(t)q(\tau)p(\tau)-p^*(\tau)p^2(t)q(\tau) \\
&\qquad\qquad +\kappa^2 q^2(t)q(\tau)p(\tau)-(-1)^{(n_1+n_2)}\kappa^2 q^2(t)p^*(\tau)q(\tau)\Big\}\Big]e^{i\omega_n(t-\tau)}. \qquad \text{(A3)}
\end{aligned}
$$

By interchanging the arguments t and τ of $\tilde{H}_I^L$ in Eq. (A3), one obtains the expression for the third term:

$$\sum_n{}'\langle 10|\,{}_{ph}\langle n|\tilde{H}_I^L(\tau)|0\rangle_{ph}\tilde{\rho}_s(t)_{ph}\langle 0|\tilde{H}_I^L(t)|n\rangle_{ph}|01\rangle$$
$$= \kappa^2\sum_n{}' C_n\Big[\kappa^2\langle 10|\tilde{\rho}_s(t)|01\rangle\Big\{(-1)^{(n_1+n_2)}q(\tau)q(t)p(\tau)p(t) - q(\tau)p^*(t)p(\tau)q(t)$$
$$- p^*(\tau)q(t)q(\tau)p(t) + (-1)^{(n_1+n_2)}p^*(\tau)p^*(t)q(\tau)q(t)\Big\}$$
$$+ \langle 01|\tilde{\rho}_s(t)|10\rangle\Big\{(-1)^{(n_1+n_2)}p^2(\tau)p^2(t) + \kappa^2p^2(\tau)q^2(t)$$
$$+ \kappa^2q^2(\tau)p^2(t) + (-1)^{(n_1+n_2)}\kappa^4q^2(\tau)q^2(t)\Big\}$$
$$+ i\kappa\langle 10|\tilde{\rho}_s(t)|10\rangle\Big\{ - (-1)^{(n_1+n_2)}q(\tau)p^2(t)p(\tau) - \kappa^2q(\tau)q^2(t)p(\tau)$$
$$+ p^*(\tau)p^2(t)q(\tau) + (-1)^{(n_1+n_2)}\kappa^2p^*(\tau)q^2(t)q(\tau)\Big\}$$
$$+ i\kappa\langle 01|\tilde{\rho}_s(t)|01\rangle\Big\{(-1)^{(n_1+n_2)}p^2(\tau)q(t)p(t) - p^*(t)p^2(\tau)q(t)$$
$$+ \kappa^2q^2(\tau)q(t)p(t) - (-1)^{(n_1+n_2)}\kappa^2q^2(\tau)p^*(t)q(t)\Big\}\Big]e^{-i\omega_n(t-\tau)}. \tag{A4}$$

Lastly, we get the following fourth term:

$$\sum_n{}'\langle 10|\tilde{\rho}_s(t)_{ph}\langle 0|\tilde{H}_I^L(\tau)|n\rangle_{ph}\;{}_{ph}\langle n|\tilde{H}_I^L(t)|0\rangle_{ph}|01\rangle$$
$$= \kappa^2\sum_n{}' C_n\Big[\langle 10|\tilde{\rho}_s(t)|01\rangle\Big\{p(t)p(t-\tau)p^*(\tau) + (-1)^{(n_1+n_2)}\kappa^2q(t)q(t-\tau)p^*(\tau)$$
$$- \kappa^2(-1)^{(n_1+n_2)}p(t)q(t-\tau)q(\tau) + \kappa^2q(t)p^*(t-\tau)q(\tau)\Big\}$$
$$+ i\kappa\langle 10|\tilde{\rho}_s(t)|10\rangle\Big\{p(t)p(t-\tau)q(\tau) + (-1)^{(n_1+n_2)}\kappa^2q(t)q(t-\tau)q(\tau)$$
$$+ (-1)^{(n_1+n_2)}p(t)q(t-\tau)p(\tau) - q(t)p^*(t-\tau)p(\tau)\Big\}\Big]e^{i\omega_n(t-\tau)}. \tag{A5}$$

When $|\kappa| \ll |\Delta\varepsilon|$ one can write [using the definition of $q(t)$ in the main text]

$$\kappa q(t) \approx 2\frac{\kappa}{\Delta\varepsilon}\sin(\frac{\Delta\varepsilon}{2}t) \ll 1. \tag{A6}$$

So, for all practical purposes, one can neglect terms involving κq in Eqs. (A2)–(A5). Moreover, based on Eqs. (48) and (49), we can write

$$p(t) \approx e^{i\frac{\Delta\varepsilon}{2}t}. \tag{A7}$$

By implementing the above approximations, one can write Eqs. (A2)–(A5) as

$$\sum_n{}'\langle 10|_{ph}\langle 0|\tilde{H}_I^L(t)|n\rangle_{ph}\;{}_{ph}\langle n|\tilde{H}_I^L(\tau)|0\rangle_{ph}\tilde{\rho}_s(t)|01\rangle \approx \kappa^2\sum_n{}' C_n\langle 10|\tilde{\rho}_s(t)|01\rangle e^{i\Delta\varepsilon(t-\tau)}e^{-i\omega_n(t-\tau)}, \tag{A8}$$

$$\sum_n{}'\langle 10|\,{}_{ph}\langle n|\tilde{H}_I^L(t)|0\rangle_{ph}\tilde{\rho}_s(t)_{ph}\langle 0|\tilde{H}_I^L(\tau)|n\rangle_{ph}|01\rangle \approx \kappa^2\sum_n{}' C_n\langle 01|\tilde{\rho}_s(t)|10\rangle(-1)^{(n_1+n_2)}e^{i\Delta\varepsilon(t+\tau)}e^{i\omega_n(t-\tau)}, \tag{A9}$$

$$\sum_n{}'\langle 10|\,{}_{ph}\langle n|\tilde{H}_I^L(\tau)|0\rangle_{ph}\tilde{\rho}_s(t)_{ph}\langle 0|\tilde{H}_I^L(t)|n\rangle_{ph}|01\rangle \approx \kappa^2\sum_n{}' C_n\langle 01|\tilde{\rho}_s(t)|10\rangle(-1)^{(n_1+n_2)}e^{i\Delta\varepsilon(t+\tau)}e^{-i\omega_n(t-\tau)}, \tag{A10}$$

and

$$\sum_n{}' \langle 10|\tilde{\rho}_s(t)_{ph}\langle 0|\tilde{H}_I^L(\tau)|n\rangle_{ph}\ {}_{ph}\langle n|\tilde{H}_I^L(t)|0\rangle_{ph}|01\rangle \approx \kappa^2 \sum_n{}' C_n \langle 10|\tilde{\rho}_s(t)|01\rangle e^{i\Delta\varepsilon(t-\tau)} e^{i\omega_n(t-\tau)}, \tag{A11}$$

respectively.

Next, the differential equation for the excited state population $\langle 10|\rho_s(t)|10\rangle$ is written as

$$\begin{aligned}\frac{d\langle 10|\tilde{\rho}_s(t)|10\rangle}{dt} = -\sum_n \int_0^t d\tau \Big[& \langle 10|_{ph}\langle 0|\tilde{H}_I^L(t)|n\rangle_{ph}\ {}_{ph}\langle n|\tilde{H}_I^L(\tau)|0\rangle_{ph}\tilde{\rho}_s(t)|10\rangle \\ & - \langle 10|\ {}_{ph}\langle n|\tilde{H}_I^L(t)|0\rangle_{ph}\tilde{\rho}_s(t)_{ph}\langle 0|\tilde{H}_I^L(\tau)|n\rangle_{ph}|10\rangle \\ & - \langle 10|\ {}_{ph}\langle n|\tilde{H}_I^L(\tau)|0\rangle_{ph}\tilde{\rho}_s(t)_{ph}\langle 0|\tilde{H}_I^L(t)|n\rangle_{ph}|10\rangle \\ & + \langle 10|\tilde{\rho}_s(t)_{ph}\langle 0|\tilde{H}_I^L(\tau)|n\rangle_{ph}\ {}_{ph}\langle n|\tilde{H}_I^L(t)|0\rangle_{ph}|10\rangle \Big]. \end{aligned} \tag{A12}$$

In the integrand of the above equation, we express the first term as

$$\begin{aligned}&\sum_n{}' \langle 10|_{ph}\langle 0|\tilde{H}_I^L(t)|n\rangle_{ph}\ {}_{ph}\langle n|\tilde{H}_I^L(\tau)|0\rangle_{ph}\tilde{\rho}_s(t)|10\rangle \\ &= \kappa^2 \sum_n{}' C_n \Big[\langle 10|\tilde{\rho}_s(t)|10\rangle \Big\{ p(t)p(t-\tau)p^*(\tau) + (-1)^{(n_1+n_2)}\kappa^2 q(t)q(t-\tau)p^*(\tau) \\ &\qquad + \kappa^2 q(t)p^*(t-\tau)q(\tau) - (-1)^{(n_1+n_2)}\kappa^2 p(t)q(t-\tau)q(\tau) \Big\} \\ &\quad - i\kappa\langle 01|\tilde{\rho}_s(t)|10\rangle \Big\{ p(t)p(t-\tau)q(\tau) + \kappa^2(-1)^{(n_1+n_2)} q(t)q(t-\tau)q(\tau) \\ &\qquad - q(t)p^*(t-\tau)p(\tau) + (-1)^{(n_1+n_2)} p(t)q(t-\tau)p(\tau) \Big\} \Big] e^{-i\omega_n(t-\tau)}, \end{aligned} \tag{A13}$$

the second term as

$$\begin{aligned}&\sum_n{}' \langle 10|\ {}_{ph}\langle n|\tilde{H}_I^L(t)|0\rangle_{ph}\tilde{\rho}_s(t)_{ph}\langle 0|\tilde{H}_I^L(\tau)|n\rangle_{ph}|10\rangle \\ &= \kappa^2 \sum_n{}' C_n \Big[\kappa^2 \langle 10|\tilde{\rho}_s(t)|10\rangle \Big\{ p(t)p^*(\tau)q(t)q(\tau) - (-1)^{(n_1+n_2)} p(t)q(\tau)q(t)p(\tau) \\ &\qquad - (-1)^{(n_1+n_2)} q(t)p^*(\tau)p^*(t)q(\tau) + q(t)q(\tau)p^*(t)p(\tau) \Big\} \\ &\quad + \langle 01|\tilde{\rho}_s(t)|01\rangle \Big\{ p^2(t)p^{*\ 2}(\tau) + (-1)^{(n_1+n_2)}\kappa^2 p^2(t)q^2(\tau) \\ &\qquad + (-1)^{(n_1+n_2)}\kappa^2 q^2(t)p^{*\ 2}(\tau) + \kappa^4 q^2(t)q^2(\tau) \Big\} \\ &\quad + i\kappa\langle 10|\tilde{\rho}_s(t)|01\rangle \Big\{ -p(t)p^{*\ 2}(\tau)q(t) - (-1)^{(n_1+n_2)}\kappa^2 p(t)q^2(\tau)q(t) \\ &\qquad + (-1)^{(n_1+n_2)} q(t)p^{*\ 2}(\tau)p^*(t) + \kappa^2 q(t)q^2(\tau)p^*(t) \Big\} \\ &\quad + i\kappa\langle 01|\tilde{\rho}_s(t)|10\rangle \Big\{ p^2(t)p^*(\tau)q(\tau) - (-1)^{(n_1+n_2)} p^2(t)q(\tau)p(\tau) \\ &\qquad + (-1)^{(n_1+n_2)}\kappa^2 q^2(t)p^*(\tau)q(\tau) - \kappa^2 q^2(t)q(\tau)p(\tau) \Big\} \Big] e^{i\omega_n(t-\tau)}, \end{aligned} \tag{A14}$$

the third term as

$$\begin{aligned}
&\sum_n{}'\langle 10|\ {}_{ph}\langle n|\tilde{H}_I^L(\tau)|0\rangle_{ph}\tilde{\rho}_s(t)_{ph}\langle 0|\tilde{H}_I^L(t)|n\rangle_{ph}|10\rangle \\
&= \kappa^2\sum_n{}' C_n\Big[\kappa^2\langle 10|\tilde{\rho}_s(t)|10\rangle\Big\{p(\tau)p^*(t)q(\tau)q(t) - (-1)^{(n_1+n_2)}p(\tau)q(t)q(\tau)p(t) \\
&\qquad\qquad - (-1)^{(n_1+n_2)}q(\tau)p^*(t)p^*(\tau)q(t) + q(\tau)q(t)p^*(\tau)p(t)\Big\} \\
&\quad + \langle 01|\tilde{\rho}_s(t)|01\rangle\Big\{p^2(\tau)p^{*\ 2}(t) + (-1)^{(n_1+n_2)}\kappa^2p^2(\tau)q^2(t) \\
&\qquad\qquad + (-1)^{(n_1+n_2)}\kappa^2q^2(\tau)p^{*\ 2}(t) + \kappa^4q^2(\tau)q^2(t)\Big\} \\
&\quad + i\kappa\langle 10|\tilde{\rho}_s(t)|01\rangle\Big\{ - p(\tau)p^{*\ 2}(t)q(\tau) - (-1)^{(n_1+n_2)}\kappa^2p(\tau)q^2(t)q(\tau) \\
&\qquad\qquad + (-1)^{(n_1+n_2)}q(\tau)p^{*\ 2}(t)p^*(\tau) + \kappa^2q(\tau)q^2(t)p^*(\tau)\Big\} \\
&\quad + i\kappa\langle 01|\tilde{\rho}_s(t)|10\rangle\Big\{p^2(\tau)p^*(t)q(t) - (-1)^{(n_1+n_2)}p^2(\tau)q(t)p(t) \\
&\qquad\qquad + (-1)^{(n_1+n_2)}\kappa^2q^2(\tau)p^*(t)q(t) - \kappa^2q^2(\tau)q(t)p(t)\Big\}\Big]e^{-i\omega_n(t-\tau)},
\end{aligned} \tag{A15}$$

and the fourth term as

$$\begin{aligned}
&\sum_n{}'\langle 10|\tilde{\rho}_s(t)_{ph}\langle 0|\tilde{H}_I^L(\tau)|n\rangle_{ph}\ {}_{ph}\langle n|\tilde{H}_I^L(t)|0\rangle_{ph}|10\rangle \\
&= \kappa^2\sum_n{}' C_n\Big[\langle 10|\tilde{\rho}_s(t)|10\rangle\Big\{p^*(t)p^*(t-\tau)p(\tau) + (-1)^{(n_1+n_2)}\kappa^2q(t)q(t-\tau)p(\tau) \\
&\qquad\qquad - (-1)^{(n_1+n_2)}\kappa^2q(\tau)q(t-\tau)p^*(t) + \kappa^2q(t)p(t-\tau)q(\tau)\Big\} \\
&\quad + i\kappa\langle 10|\tilde{\rho}_s(t)|01\rangle\Big\{p^*(t)p^*(t-\tau)q(\tau) + (-1)^{(n_1+n_2)}\kappa^2q(t)q(t-\tau)q(\tau) \\
&\qquad\qquad + (-1)^{(n_1+n_2)}q(t-\tau)p^*(t)p^*(\tau) - q(t)p(t-\tau)p^*(\tau)\Big\}\Big]e^{i\omega_n(t-\tau)}.
\end{aligned} \tag{A16}$$

When $|\kappa| \ll |\Delta\varepsilon|$, we can simplify Eqs. (A13)–(A16) as

$$\sum_n{}'\langle 10|_{ph}\langle 0|\tilde{H}_I^L(t)|n\rangle_{ph}\ {}_{ph}\langle n|\tilde{H}_I^L(\tau)|0\rangle_{ph}\tilde{\rho}_s(t)|10\rangle \approx \kappa^2\sum_n{}' C_n\langle 10|\tilde{\rho}_s(t)|10\rangle e^{i\Delta\varepsilon(t-\tau)}e^{-i\omega_n(t-\tau)}, \tag{A17}$$

$$\sum_n{}'\langle 10|\ {}_{ph}\langle n|\tilde{H}_I^L(t)|0\rangle_{ph}\tilde{\rho}_s(t)_{ph}\langle 0|\tilde{H}_I^L(\tau)|n\rangle_{ph}|10\rangle \approx \kappa^2\sum_n{}' C_n\Big(1 - \langle 10|\tilde{\rho}_s(t)|10\rangle\Big)e^{i\Delta\varepsilon(t-\tau)}e^{i\omega_n(t-\tau)}, \tag{A18}$$

$$\sum_n{}'\langle 10|\ {}_{ph}\langle n|\tilde{H}_I^L(\tau)|0\rangle_{ph}\tilde{\rho}_s(t)_{ph}\langle 0|\tilde{H}_I^L(t)|n\rangle_{ph}|10\rangle \approx \kappa^2\sum_n{}' C_n\Big(1 - \langle 10|\tilde{\rho}_s(t)|10\rangle\Big)e^{-i\Delta\varepsilon(t-\tau)}e^{-i\omega_n(t-\tau)}, \tag{A19}$$

and

$$\sum_n{}'\langle 10|\tilde{\rho}_s(t)_{ph}\langle 0|\tilde{H}_I^L(\tau)|n\rangle_{ph}\ {}_{ph}\langle n|\tilde{H}_I^L(t)|0\rangle_{ph}|10\rangle \approx \kappa^2\sum_n{}' C_n\langle 10|\tilde{\rho}_s(t)|10\rangle e^{-i\Delta\varepsilon(t-\tau)}e^{i\omega_n(t-\tau)}, \tag{A20}$$

respectively. The multimode case can be derived in a similar fashion by replacing ω_n, C_n, κ, and n_i with $\bar{\omega}_n$, $\bar{C}_n$, $\bar{\kappa}$, and $\sum_k n_i^k$, respectively.

[1] M. A. Nielsen and I. Chuang, *Quantum Computation and Quantum Communication* (Cambridge University Press, Cambridge, 2000).

[2] M. Schlosshauer, Rev. Mod. Phys. **76**, 1267 (2005).
[3] W. H. Zurek, Rev. Mod. Phys. **75**, 715 (2003).
[4] H. J. Lipkin, N. Meshkov, and A. J. Glick , Nucl. Phys. **62**, 188 (1965).
[5] S. Morrison and A. S. Parkins, Phys. Rev. A **77**, 043810 (2008); Phys. Rev. Lett. **100**, 040403 (2008).
[6] M. Ezawa, New J. of Phys. **11** 095005 (2009); Phys. Rev. B **79**, 241407(R) (2009).
[7] G. S. Engel, T. R. Calhoun, E. L. Read, T-K Ahn, T. Mancal T, Y-C Cheng, R. E. Blankenship, and G. R. Fleming, Nature **446**, 782 (2007).
[8] Y-C. Cheng and G. R. Fleming, Annu. Rev. Phys. Chem. **60**, 241 (2009).
[9] A. W. Chin, A. Datta, F. Caruso, S. F. Huelga, and M. B. Plenio, New J. Phys. **12**, 065002 (2010).
[10] For a study of coherence in semiconductor DQDs, see J. R. Petta, A. C. Johnson, J. M. Taylor, E. A. Laird, A. Yacoby, M. D. Lukin, C. M. Marcus, M. P. Hanson, and A. C. Gossard, Science **309**, 2180 (2005); and H. Bluhm, S. Foletti, I. Neder, M. Rudner, D. Mahalu, V. Umansky, and A. Yacoby, Nature Physics **7**, 109 (2011).
[11] L -A. Wu and D. A. Lidar, Phys. Rev. Lett. **91**, 097904 (2003).
[12] A. Dey and S. Yarlagadda, Phys. Rev. B **89**, 064311 (2014).
[13] I. G. Lang and Y. A. Firsov, Zh. Eksp. Teor. Fiz. **43**, 1843 (1962) [Sov. Phys. JETP **16**, 1301 (1963)].
[14] S. Datta, A. Das, and S. Yarlagadda, Phys. Rev. B **71**, 235118 (2005).
[15] Strong coupling occurs quite commonly in transition metal oxides such as manganites; see A. Lanzara, N. L. Saini, M. Brunelli, F. Natali, A. Bianconi, P. G. Radaelli, and S -W. Cheong Phys. Rev. Lett. **81**, 878 (1998); A. J. Millis, P. B. Littlewood, and B. I. Shraiman, Phys. Rev. Lett. **74**, 5144 (1995); and Ref. 14. As mentioned in Ref. 12, for manganites $6 < g^2 < 10$.
[16] Nonadiabaticity occurs in systems such as C60 compounds; see L. Pietronero, S. Strssler, and C. Grimaldi, Phys. Rev. B **52**, 10516 (1995).
[17] S. Datta and S. Yarlagadda, Solid State Commun. **150**, 2040 (2010).
[18] Sahinur Reja, Sudhakar Yarlagadda, and Peter B. Littlewood, Phys. Rev. B **84**, 085127 (2011).
[19] S. Reja , S. Yarlagadda, and P. B. Littlewood, Phys. Rev. B **86**, 045110 (2012).
[20] J. R. Schrieffer and P. A. Wolff, Phys. Rev. **149**, 491 (1966).
[21] S. Bravyi, D. DiVincenzo and D. Loss, Ann. Phys. **326**, 2793 (2011).
[22] A. Dey, M. Q. Lone and S. Yarlagadda (unpublished).
[23] R. Pankaj and S. Yarlagadda, Phys. Rev. B **86**, 035453 (2012).
[24] For a large N system, the largest energy contribution due to terms involving closed loops is intensive. The dominant contribution, in second and higher order perturbation, comes from open loops. The approximate open loop terms in zeroth, second, and third order perturbation are, respectively, $J_\perp e^{-g^2}\sum_{i,j\neq i} b_i^\dagger b_j$, $[NJ_\perp^2 e^{-g^2}/(g^2\omega)]\sum_{i,j\neq i} b_i^\dagger b_j$, and $[N^2 J_\perp^3 e^{-g^2}/(g^2\omega)^2]\sum_{i,j\neq i} b_i^\dagger b_j$; then, the small parameter is $J_\perp^\star/(g^2\omega)$.
[25] H. P. Beuer and F. Petruccione, *The Theory of Open Quantum systems* (Oxford University Pres, Oxford, New York, 2002).
[26] K. Modi, Nature Scientific Reports **2**, 581 (2012).
[27] V. G. Morozov, S. Mathey and G. Röpke, Phys. Rev. A **85**, 022101 (2012).
[28] H. J. Carmichael, *S*tatistical Methods in Quantum Optics I (Springer-Verlag, Berlin, 2008).
[29] C. Meier and D. J. Tannor, J. Chem. Phys. **111**, 3365 (1999).
[30] Y. J. Yan, Phys. Rev. A **58**, 2721 (1998).
[31] R. X. Xu and Y. J. Yan, J. Chem. Phys. **114**, 3868 (2001).
[32] H. P. Breuer, B. Kappler and F. Petruccione, Phys. Rev. A **59**, 1633 (1999).
[33] H. P. Breuer, B. Kappler, and F. Petruccione, Ann. Phys. (NY) **291**, 36 (2001).
[34] M. Schröder, U. Kleinekathöfer, and M. Schreiber, J. Chem. Phys. **124**, 084903 (2006).
[35] E. Ferraro, M. Scala, R. Migliore and A. Napoli, Phys. Rev. A **80**, 042112 (2009).
[36] H. S. Goan, P. W. Chen, and C. C. Jian, J. Chem. Phys. **134**, 124112 (2011).
[37] U. Kleinekathöfer, J. Chem. Phys. **121**, 2505 (2004).
[38] R. Roth and K. Burnett, Phys. Rev. A **68**, 023604 (2003).
[39] Our analysis of the case with $\Delta\varepsilon = 0$ is consistent with the findings (of nearly adiabatic evolution in a polaron band at strong coupling in the Holstein model) in L. Vidmar, J. Bonča, M. Mierzejewski, P. Prelovšek, and S. A. Trugman, Phys. Rev. B **83**, 134301 (2011).

Appendix B: Popular Summary

Photosynthesis is a process used by plants and other organisms to convert light into the chemical energy used by most life on earth. Understanding the highly efficient transport of absorbed light-energy through molecules in photosynthesis is of significant scientific interest and also key to designing light-harvesting technology. Surprisingly, experiments reveal that superposition principle of quantum mechanics plays a crucial role in this biological transport process; it is the interference of the superposed states (much like the interference in waves) and its preservation during transport that is key to the high efficiency of the process. However, the precise features that preserve the quantum interference during transport have remained elusive. Next, also of immense interest is the successful exploitation of quantum mechanics for quantum computation so as to solve complex problems that are intractable by present-day classical computers. A qubit is the building block of a quantum computer much like a bit in a classical computer. Superposition principle is what distinguishes a quantum bit (qubit) from a classical bit. Although a few promising candidates for a qubit exist, none of them preserve superposition of the two states of a qubit for extended time periods. Unfortunately, interaction of the excited molecules (in photosynthesis) and qubits (in a quantum computer) with the ubiquitous environmental noise is inevitable; this coupling to noise can degrade the superposition of states in a system of molecules or a qubit, i.e., can produce decoherence in them. Our work identifies a few key features that reduce decoherence significantly.

The excitations in photosynthesis and the qubit in quantum computation can be modeled by a spin or a hard-core boson (HCB), i.e., a boson that does not allow another one to occupy the same site. Crucially, the system and the environment (comprising of optical phonons) should be initially uncorrelated in the frame of reference where the HCB is dressed by the deformation it produces in the lattice environment. Our work shows that coherence is maximized if HCBs have distance-independent hopping in a lattice. Furthermore, if each site in the lattice has a different potential, then coherence is preserved when the potential differences between sites is as far away as possible from any of the environmental eigenenergies (and particularly those close to twice the lattice deformation energy). Interestingly, we show that the stronger the HCB couples with the environment, the lesser is the decoherence.

Thus, our work would help in developing synthetic light-absorbing materials with efficient energy transfer as well as in realizing charge qubits with small decoherence. An oxide- (i.e., manganite-) based double quantum dot can serve as a robust charge qubit and meet the demands put by miniaturization on computer technology.